Nano Research 2018, 11(10): 5372–5399
https://doi.org/10.1007/s12274-018-2189-3
Review Article
ISSN 1998-0124
CN 11-5974/O4

Nanobiotechnology: 1D nanomaterial building blocks for cellular interfaces and hybrid tissues

Haitao Liu[1,2,§], Bilal Haider[1,§], Holden R. Fried[1,§], Jie Ju[1], Olurotimi Bolonduro[1], Vineeth Raghuram[1], and Brian P. Timko[1] (✉)

[1] *Department of Biomedical Engineering, Tufts University, Medford, Massachusetts 02155, USA*
[2] *School of Materials Science and Technology, China University of Geosciences, Beijing 100083, China*
[§] *Haitao Liu, Bilal Haider and Holden R. Fried contributed equally to this work.*

Received: 29 May 2018
Revised: 28 August 2018
Accepted: 2 September 2018

KEYWORDS
nanomaterial,
neuron,
cardiomyocyte,
nanoelectronics,
bioelectronics,
hybrid tissue

ABSTRACT

Solid-state nanomaterials exhibit complementary interactions with biological systems because of their biologically-relevant size scales and rationally tunable electrical, chemical and mechanical properties. In this review, we focus specifically on one-dimensional (1D) nanomaterials such as silicon or gold nanowires or carbon nanotubes. We discuss the nature of the nanomaterial–cell interface, and how that interface may be engineered to enhance or modulate cellular function. We then describe how those unique interfaces may be exploited in three-dimensional (3D) tissue culture to recapitulate the extracellular matrix and promote or complement morphogenesis. Finally, we describe how 1D nanomaterials may be elucidated as nanoelectronic devices that monitor the chemical or electrical environment of cells or tissue with exquisite spatial and temporal resolution. We discuss prospects for entirely new classes of engineered, hybrid tissues with rationally-designed biological function and two-way, closed-loop electronic communication.

1 Introduction

Recent advances in nanoscience and nanotechnology have enabled entirely new modalities for interacting with biological systems, leading to advances in drug delivery [1, 2], tissue engineering [3, 4], biomedical imaging [5] and bioelectronics [6, 7]. Nanomaterials—structures defined as having at least one critical dimension in the 1–100 nm regime—exhibit numerous properties that make them amenable for use in biological systems. In some contexts, they may be considered biomimetic. They exhibit a size scale that is on the order of many biological features, including the hydrodynamic radius of a protein or the nanotopography of the extracellular matrix (ECM). They also exhibit a high surface-area-to-volume ratio and rich surface chemistry and so may be imbued chemical functionalities to confer desired characteristics,

Address correspondence to brian.timko@tufts.edu

ranging from immune evasion (e.g. "stealth" nanoparticles) to receptor-targeting. Moreover, because of quantum confinement effects, nanomaterials may exhibit optical, electrical or magnetic properties that are unachievable in bulk systems. These unique characteristics have been exploited to achieve a variety of functions in biological systems, ranging from externally-triggered drug delivery [2] to biosensing [6].

In this review, we will focus specifically on 1D nanomaterials, defined as structures that are nanoconfined in two directions and typically microns long in the third. While these structures have been achieved as both soft [8] and solid-state [9, 10] materials, we will here focus on the latter, with a specific emphasis on silicon nanowires (SiNWs), gold nanowires (AuNWs) and carbon nanotubes (CNTs). We chose to focus on 1D nanomaterials because of their inherent anisotropy, which is relevant to biological systems given that the ECM is itself nanofibrous—and in many cases anisotropic on a micro- or macro-scale as well [3]. Their electrical properties—ranging from insulating to metallic—are also relevant, as they may form interconnected networks throughout tissues or other biological constructs enabling electrotonic distribution of electric fields, including those incorporating scaffolds that are polymeric and otherwise insulating. This property is particularly relevant in the areas of nerve and muscle tissue engineering, where electric fields are necessary to mediate biological function, including morphogenesis [11]. Finally, 1D nanomaterials may function as building blocks in nanoelectronic devices, either as elements of multi-electrode arrays (MEAs) or as the active channel in a field-effect transistor (FET). In either case, these materials offer access not only to extracellular spaces but also to the cytosol of electrically-active cells, enabling multiple modalities for electrophysiological measurements.

1D nanomaterials offer a compelling route toward hybrid tissues—that is, constructs that seamlessly integrate engineered tissues with solid-state components. We will discuss the interactions between these two disparate but complementary systems first at the level of fundamental cell/nanomaterial interfaces, then within the context of three-dimensional (3D) engineered tissues. We will then discuss the field of nanoelectronics, including how nanoelectronic devices may be implemented to probe the state of a tissue by providing multiplexed readouts with high spatial and temporal resolution. Collectively, these 1D nanomaterial interfaces are likely to enable hybrid tissues that mimic and extend the function of their endogenous counterparts, representing a platform for fundamental studies, diagnostics, and regenerative medicine.

2 Nanomaterial interactions at the cellular level

Nanomaterials and nanostructured surfaces offer a plethora of unique features that have been exploited to enhance cellular adhesion, modulate function, and increase biocompatibility. Many of these features have been realized within the context of implantable macro- or microscale devices [12]. For example, nanostructured coatings on the surface of neural electrode implants reduced inflammatory response, improved electrical coupling, and enabled smaller electrodes that could interface with tissues while providing greater spatial resolution. Yet despite their clear utility, the fundamental nature of cell/nanomaterial interfaces is still an area of intense research. Interactions are complex and depend on the geometry and orientation of the nanomaterial as well as its surface chemistry, which may evolve over time as a protein corona forms. The complexity of the cell membrane—presenting cell-specific combinations of lipids, proteins and carbohydrates—introduces additional complexity. Approaches to understand these interactions have been explored at scales ranging from long-range (e.g., van der Waals interactions) to short-range (e.g., protein-specific binding), and have been reviewed in depth [13, 14].

2.1 Functionalization and surface chemistry

Given their high surface-to-volume ratio, the surface chemistry of nanomaterials plays a substantial role in dictating cellular interactions [14]. Methods to achieve self-assembled monolayers (SAMs) on oxide [15], metal [16] and sp^2-hybridized carbon [17] surfaces have been widely explored, initially within the context of planar surfaces and more recently with respect to nanomaterials. These surface chemistries have enabled

rich control of the wettability and charge of the nanomaterial, and have also enabled conjugation of biomolecules that promote membrane-specific interactions, e.g. to integrin receptors [18].

Nanotopography—achievable, for example, by a mat or vertical array of 1D nanomaterials—enables regimes of superhydrophilicity (contact angle $\theta \approx 0°$ [19]) or superhydrophobicity ($\theta > 150°$) not typically achievable by planar surfaces. Poly(ethylene glycol) (PEG), a widely-studied moiety that inhibits protein and cellular attachment [16, 20], typically exhibits $\theta \approx 45°$ on planar surfaces [21]; the same moiety on nanoporous surfaces confers superhydrophilicity, as does ozone treatment [22]. Conversely, SAMs of alkane [23] or perfluorocarbon ligands [24] impart hydrophobicity at most in the range $\theta = 100°–120°$ on planar surfaces, but as high as $\theta = 152°$ on SiNW mats [25]. One model to describe these phenomena is represented by Wenzel's equation

$$\cos \theta' = r \cdot \cos \theta \quad (1)$$

where the apparent contact angle of a surface (θ') is a function of the roughness factor (r) [19, 26]. While this model holds for both superhydrophilic and superhydrophobic surfaces, it assumes that the surface is fully wetted by the solvent. Cassie and Baxter proposed a different model for superhydrophobic surfaces whereby liquid does not intrude into the nanoscale pores, and so only a small fraction is in contact with the substrate. To describe the relationship between the apparent and the intrinsic contact angle in this partially-wet state, a modified Cassie-Baxter equation

$$\cos \theta' = f \cdot \cos \theta - (1 - f) \quad (2)$$

is sometimes applied, where f is the fraction of solid in contact with the liquid. Since f is generally small for nanostructured surfaces, surfaces in a Cassie-Baxter state are ideal for preventing protein or cellular adhesion [27].

Superhydrophilic or superhydrophobic surfaces based on 1D materials may be considered biomimetic given the hierarchical nature of water- or oil-repellent structures found in plants and animals [28]. These properties have been useful *in vitro*, as benign epithelial (MCF-10A), cancer (HeLa) or Chinese hamster ovary cells have been patterned on diamond nanowires (NWs) [22] or SiNWs [29] with defined superhydrophobic domains. In both studies, superhydrophilic domains promoted cellular attachment, and other studies showed that nanoscale chemical heterogeneity promoted neuronal adhesion and differentiation [30]. These unique effects may be due to the ability of nanoscale features to direct focal adhesion (FA) formation, as will be discussed in Section 2.4.

The surface charge of a nanomaterial is another crucial component in biomedical applications, since cell membranes preferentially adhere to positively-charged surfaces [14]. Nanomaterials may amplify surface charge, as was reported for nanostructured surfaces functionalized with carboxyl (–COOH) or amino ($–NH_2$) groups that suppressed or enhanced attachment of epithelial cells compared to similarly-modified planar substrates [31]. Studies of HepG2, Caski, and MCF-7 cancer cell lines on ZnO NW arrays demonstrated that cytotoxicity was charge-dependent [32]. Negatively-charged nanoparticles interacted exclusively with excitable neurons, depolarizing their membrane and enhancing excitability, although the phenomenon was size-, shape- and material-dependent [33].

2.2 Tight junctions

Nanostructures have been shown to form extraordinarily tight junctions with cell membranes. CNTs, either as discrete nanostructures or mats, have been widely explored in this context [34]. CNTs interfaced with supported lipid bilayers—used as models for cell membranes—blocked diffusion of glycolipid-bound toxins without inhibiting the intrinsic fluidity of the bilayer. This observation implied a CNT–membrane junction with critical feature size on the order of or smaller than the size of the toxin [35]. Transmission electron microscopy (TEM) of junctions between CNTs and hippocampal neurons demonstrated an even more intimate interface where the CNTs "pinched" the membrane to form discontinuous regions of tight junctions [36]. Similar phenomena were also observed with neurons grown on mats of interconnected CNTs, where scanning electron microscopy (SEM) showed

that neuronal processes were distorted by, and tightly adhered to, CNT bundles (Fig. 1(a)) [37].

Similar tight junctions have also been observed from neurons cultured on gold nanopillar arrays, which could be fabricated with independent control over spacing, height and diameter. TEM or focused ion beam SEM (FIB-SEM) analysis demonstrated that cellular interactions were highly dependent upon the geometry of those arrays [39]. For example, in the case of closely spaced pillars with diameter < 300 nm, the membranes of HL-1 cells conformed to the shape of the nanopillars, fully wrapping around the entirely of the tip (Fig. 1(b)). Similar effects were observed for large neurites (e.g. > 1 μm) from cortical neurons, which also fully engulfed the nanopillars. In either case, the cleft (membrane-to-surface distance) was typically < 20 nm, substantially less than the > 50 nm spacing observed from flat substrates. Significantly, these tight junctions were specific to protruding structures with sufficiently small diameter; in the case of nanopillars > 500 nm diameter or nanoscale invaginations (pores) rather than pillars, the cell membranes did not conform to the surface but instead remained suspended in a "bed of nails" regime with cleft > 10 times greater than for the case of small-diameter nanopillars (Figs. 1(c) and 1(d)) [38, 39].

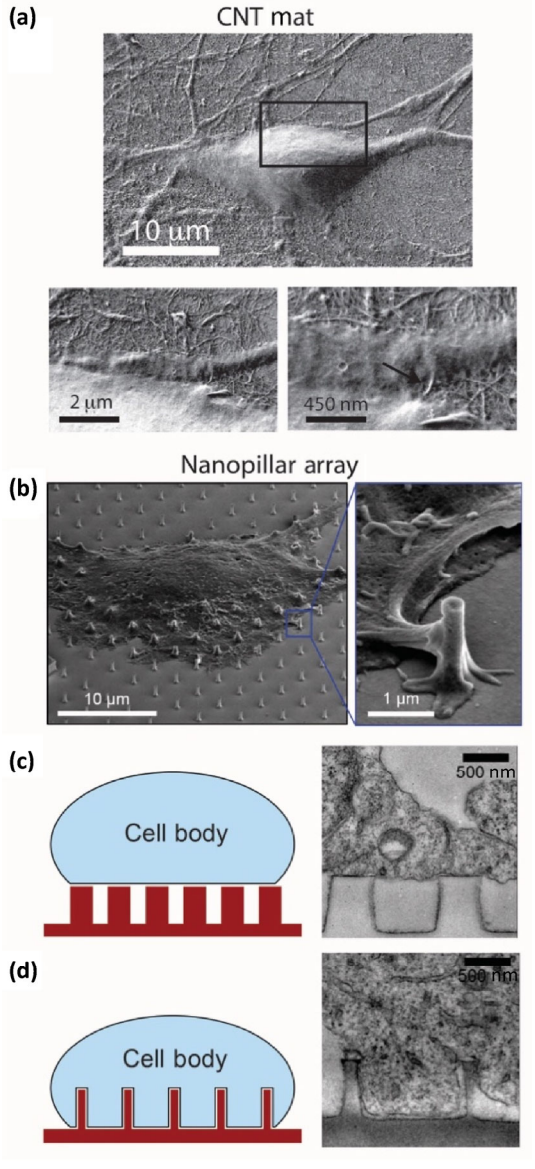

Figure 1 (a) SEM of hippocampal neurons cultured on CNT mats; insets detail framed region and (black arrow) highlight intimate contact between CNT bundles and cell membrane. (b) SEM of HL-1 cell cultured on nanopillars; inset shows membrane protrusions in contact with a nanopillar. (c) Schematic and accompanying TEM of cell body sitting atop 500 nm diameter nanopillars and (d) in tight contact with 200 nm diameter nanopillars. Adapted with permission from Ref. [37], © Society for Neuroscience 2007; Ref. [38], © American Chemical Society 2017; Ref. [39], © American Chemical Society 2012.

2.3 Electrophysiology and synaptic connectivity

Given the unique mechanical interactions just described, it may not be surprising that nanomaterial interfaces also modulate cellular electrophysiology. Compared to planar surfaces, rat hippocampal neurons grown on CNT mats showed a roughly six-fold increase in the frequency of spontaneous postsynaptic currents—indicators of functional synapse formation—as well as a roughly six-fold increase in spontaneous action potentials (APs) [40]. Interestingly, neurons grown on CNT and planar surfaces exhibited similar resting membrane potential, input resistance and capacitance, and also had similar densities and neurite lengths. These observations suggest that CNTs did not alter the properties of the membrane, but rather formed an intimate junction that could electrotonically distribute current and alter the charge along the surface of the membrane. In a separate study, researchers drew a similar conclusion, i.e., that CNTs could enhance neuronal excitability by forming shortcuts between different intracellular compartments [36]. In this study, neurons cultured on CNT mats uniquely exhibited after-depolarizations (ADPs), which are mediated by action potentials that back propagate from the soma

into the dendrites. The authors hypothesized that these effects were caused by direct electrical coupling between the soma and the dendrites through the CNT network, although the CNTs may have also contributed by potentiating calcium-mediated currents and/or by inducing channel clustering through mechanical interactions on the membrane, either of which could contribute to ADPs. Additionally, neuron pairs grown on CNT mats also showed enhanced formation of GABAergic synapses, potentially induced by back-propagating APs [41]. Notably, similar interactions were not observed from neurons grown on planar conductive indium tin oxide substrates, highlighting the important and unique role of nano-topography in neuronal electrophysiology.

CNT mats could also accelerate the development of immature rat spinal neurons. Neurons cultured on CNT mats were about twice as likely to exhibit voltage-gated currents and produce APs on day 8, before the appearance of synaptic activity. The authors hypothesized that the tight junction between neurons and CNTs triggered a cascade of intracellular signaling events leading to changes in transcriptional regulation, differentiation and survival [42].

2.4 Focal adhesions

Nanomaterials are known to modulate protein expression in cells [43]. Many of these interactions relate to formation of FAs, which link the ECM to the actin cytoskeleton and mediate cell adhesion, spreading, migration, mechanosensing and signaling. FAs are mediated by integrin binding complexes, which have a nanoscale protein organization whose configuration is crucial to the function and activity of the complex [44]. Nanostructured substrates that recapitulate the porosity and mechanical properties of the ECM are thought to present binding sites that align key integrin proteins such as vinculin and paxillin, thereby activating the FA. Such an effect was observed with mesenchymal stem cells cultured on vertically oriented TiO_2 nanotubes, where nanotubes with < 30 nm diameter presented an effective size scale for accelerated integrin clustering and FA formation compared to nanotubes with diameter > 30 nm, or planar surfaces. Cells that could not form FAs, e.g. in the case of 100 nm nanotubes where binding sites were unavailable, produced apoptosis signals that led to cell death (Fig. 2(a)) [45]. The mechanical properties of the substrate were also crucial, as HEK 293T cells cultured on vertical SiNW arrays formed more FAs to long, thin NWs since they were more readily deflected and presented more sites for FA formation, compared to stiffer samples [46].

2.4.1 *Adhesion, spreading and motility*

Vertical structures also modulate cellular motility. Early works involved "picket fences" that physically trapped neurons [47]. More recent studies have shown that nanopillar or NW arrays could pin neurons not by blocking their path but rather by preferentially inducing FA formation. This phenomenon was demonstrated with neurons cultured near rings of Pt nanopillars, where neurites were guided atop, and some cases wrapped around, the nanopillars. Pinned neurons were essentially stationary over a period of 4 days, while unpinned neurons (e.g., those on a planar surface) could migrate over a hundred microns during the same time period (Fig. 2(b)) [48]. Similar effects were observed with SiNW arrays, where cells extended filopodia to grasp the NWs and also exhibited lesser motility [49]. That effect, however, appeared to be dependent on the geometry of the NW array, as a high NW density enabled a "bed of nails" regime where cells resided atop the NWs and remained fully motile (see Section 2.2) [50].

NW arrays that decreased cellular motility also appeared to increase the force of adhesion [49] and in some cases promoted spreading [50]. Traction forces have been quantified at the single-cell level with both benign (L929) and malignant (HeLa) cells, by observing the mechanical displacement of the NWs [51]. Forces exerted by cells on NWs (or vice versa) were corelated to genotypic changes associated with mechanotransduction pathways. Integrins and focal adhesion kinase (FAK), which play a key role in transducing force from the extracellular matrix to the cellular cytoskeleton, were both upregulated; while α-actin, which is responsible for motility and structure, was downregulated [49].

As alluded to earlier, the surface chemistry of the NWs also plays a role in directing FA formation. Interestingly, hydrophobic vertical NW arrays increased

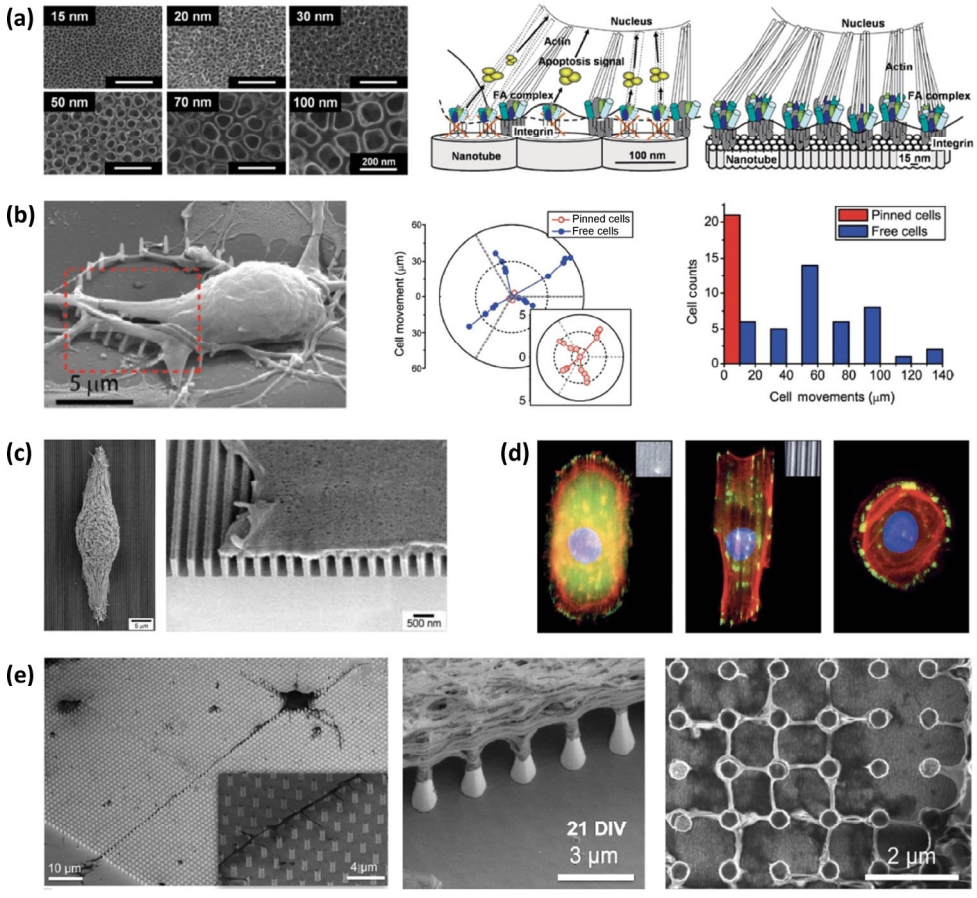

Figure 2 Nanotopography influences FAs. (a) (left) Vertically aligned TiO_2 nanotubes with different diameters and (right) schemes representing nanotopography-dependent FA activation and apoptotic signaling. (b) (left) SEM of neurites preferentially adhered to nanopillar arrays and (right) motility over 4 days for (red) pinned and (blue) free cells. (c) SEM of epithelial cells grown on nanogrooved substrates showing (left) elongation and (right) extended and guided filopodia. (d) Fluorescence images of epithelial cells showing (red) actin, (green) vinculin and (blue) nucleus, cultured on nanogrooved surfaces with (left) 400 nm pitch or (center) 4,000 nm pitch, or (right) on flat surface. (e) Cortical neurons cultured on vertical NW array: (left) single neuron 2 DIV with single polarized projection, inset shows closer view around the axon; (center) network after 21 DIV suspended on tips of NWs; (right) network after 5 DIV showing anchoring and secondary branching at the NWs. Adapted with permission from Refs. [45], © American Chemical Society 2007; Ref. [48], © American Chemical Society 2010; Ref. [52], © The Company of Biologists Ltd. 2003; Ref. [53], © American Chemical Society 2017.

adhesion and viability of mesenchymal stem cells (MSCs), but also prevented them from spreading [54]. This finding was consistent with a study of MSCs on hydrophobic TiO_2 nanotubes with contact angle > 120°, in which 100 nm-diameter tubes showed increased adhesion, but substantially less FA formation and less spreading (smaller diameters), compared to hydrophilic control [55].

2.4.2 *Alignment*

1D nanomaterials may also provide cues for cellular elongation and guidance. Nanogratings achieved as by top-down lithography or by bottom-up assembly techniques are natural candidates for this purpose, since they guide the extension of filopodia (Fig. 2(c)) and therefore direct the formation of FAs along the longitudinal direction. Alignment by this mechanism has been observed across a wide variety of cell types, including neurons, myocytes, and epithelial cells. Surface-enhanced Raman spectroscopy on cells cultured AgNW arrays demonstrated that upon alignment, the characteristic tyrosine (Tyr) peak shifted and strengthened, consistent with activation of integrin-mediated signaling pathways and FA formation [56]. These findings are consistent with fluorescence microscopy showing localization of FAs along the

nanogrooves (Fig. 2(d)) [52], as well as changes in cellular motility as described in the previous section.

Nanomaterials may alternatively direct cellular alignment by presenting periodic adhesion points; cells align along the axes of these arrays as filopodia sense the shortest distance between adjacent points. Elongation by this mechanism was in some cases observed with nanogratings just described—that is, cells extended orthogonal to the direction of nanograting [52]. Similar phenomena have also been explored with vertical NW arrays, whose geometry and periodicity could be rationally tuned. Such was the case with embryonic cortex or hippocampal neurons grown on vertical InP NW arrays, which readily extended filopodia that navigated the array, eventually adhering to adjacent NWs to form neurite extensions aligned with the array and attached at each NW. This method of polarization in some cases favored linear extensions over tens of microns (Fig. 2(e)). The authors moreover found that these engineered neural networks formed synaptic junctions, with synchronized Ca^{2+} bursts observed throughout the network [53]. Similar polarization was observed with C3H10T1/2 mesenchymal progenitor cells cultured on vertical SiNW arrays, that in some cases extended projections over hundreds of microns. Notably, this process was highly dependent on the geometry of the NW array and the stiffness of the NWs themselves. At dense (1 μm) NW pitch, cells were flat with few extensions, as the cells sat atop the NW array and filopodia were unable to navigate the surface; at moderate (2 μm) pitch, projections were highly polarized; while at large (4 μm) pitch, the cells accessed the planar substrate and were not polarized [57].

NWs have also been utilized as substrates to promote directed axonal growth of specific neuronal populations, while inhibiting the spread of others [58]. Vertically oriented GaP nanowires were used as an *in-vitro* platform for modulating the selective elongation of dissociated retinal neurons versus glial cells in a co-cultured setup, where dense 100 μm wide NW regions favored the growth of retinal cells, whereas adjacent flat regions allowed for invasion by glial cell populations. Interestingly, reductions in the width of flat regions or changes in the geometry of the NW region facilitated glial infiltration into the retinal networks [58].

2.4.3 *Stem cell differentiation*

1D nanomaterials have been shown to direct stem cell fate, which is normally affected by cytoskeletal-linked signaling pathways. Recent studies demonstrated that differentiation of neural stem cells (NSCs) into neurons was greatly increased on vertically aligned silicon nanowire arrays compared to silicon wafers [59]. This effect was evidenced by a significant increase in Tuj-1 (a commonly used neural marker for axons and dendrites) paired with a significant decrease in GFAP (a commonly used astrocytic marker) [59]. Similarly, preferential differentiation of human olfactory bulb NSCs into neurons rather than glial cells was observed when co-administering NSCs and CNTs into a rat neurodegeneration model [60].

Similar effects were leveraged to promote osteogenesis. CNT mats accelerated differentiation of hMSCs into osteoblasts, although PEGylated CNTs were more effective than carboxylated samples [61]. Hydrophobic nanopillars also initiated hMSC differentiation after promoting aggregation [54]. Consistent with studies on FAs, differentiation effects were also shown to be geometry-dependent; hMSCs cultured on TiO_2 nanotube substrates remained mostly undifferentiated in the case of 30-nm diameter tubes, but elongated and selectively differentiated into osteoblast-like cells on 70–100 nm diameter tubes [62].

2.5 Endocytosis and other forms of internalization

Methods to internalize 1D nanostructures within cells have opened entirely new avenues for modulating cellular function or monitoring the chemical or electrical environment of the cytosol [63]. 1D nanostructures are distinct from their zero-dimensional (0D) counterparts since they introduce electrical and chemical anisotropy into the system and allow for tethering to a substrate as part of a nanoelectronic device. 1D nanomaterials may be internalized by several distinct pathways including direct penetration or endocytosis, in analogy to routes already established for 0D particles [13].

One method to introduce nanomaterials into a cell is through abrasion, that is, by external application of force to disrupt the cell membrane. Freestanding NWs mounted onto micromanipulator stages have

been inserted into the cytosol in this manner. The small size of the NW, coupled with the application of an acute force, caused minimal disruption to the cell membrane, allowing the cell to remain viable for extended periods of time [64]. Membrane penetration has also been achieved via transient poration following mechanical [65], optical [66] or electrical [67, 68] stimulation. Vertical NW arrays have been successfully introduced into the cytosol in this manner, albeit for relatively short time periods, until the pores sealed and expelled the NWs from the cells. Both of these techniques have been implemented to achieve intracellular electrophysiology, which will be discussed in Section 4.2.

NWs are also capable of entering the cytosol in the absence of externally-applied forces. This principle was demonstrated with neurons cultured on vertical GaP NW arrays [69], and mouse embryonic stem (mES) cells and human embryonic kidney (HEK 293T) cells cultured on vertical SiNW arrays [70]. In the latter study, the authors noted a correlation between cellular viability and NW geometry; 400 nm diameter NWs induced cell death within a day, whereas 30 nm diameter NWs maintained viable cells for up to five days. When mES embryoid bodies were plated onto NW arrays, they differentiated into cardiomyocytes and remained viable for over one month. These findings contrast with those described in Section 2.2, where nanomaterials formed a tight junction with, but did not penetrate, the membrane. A mechanical model describing the regimes for vertical NW cell penetration has been proposed [71]. This model distinguishes between "impaling" penetration, when cells land directly onto a bed of NWs, and "adhesion-mediated" penetration, which occurs as cells spread on a surface and generate an adhesion force. The model indicates that stiffer cells have a higher penetration efficiency, but are more sensitive to NW geometry, with the likelihood of NW penetration generally anticorrelated to diameter.

Freestanding 1D nanostructures may also be internalized. In some cases, internalization occurred by endocytosis, although uptake efficiency and manner of entry were highly dependent on the size and shape of the nanoparticle [72]. CNTs were internalized by HeLa cells in this manner, and were observed within fluorescently-labeled endosomes [73]. Similarly, SiNWs activated phagocytic pathways in human umbilical vein endothelial cells (HUVECs), undergoing intracellular transport and ultimately clustering in the perinuclear region [74]. While this study reported 96% uptake, efficiency likely varies with cell type. This limitation was addressed with cell penetrating peptides (CPPs), which mediate cargo delivery by both direct penetration and endocytic pathways. SiNWs to which the CPP trans-activating transcriptional activator (TAT) had been covalently conjugated were internalized by mouse hippocampal neurons with far greater efficiency than pristine NWs [75].

2.6 Toxicity

As with all biomaterials, nanomaterials should be carefully screened for biocompatibility. Nanomaterials are especially complex, since potential toxic effects are driven not only by particle concentration, but also by size, geometry, composition and surface functionality, including the protein corona which may evolve over time. While some nanomaterials are believed to be benign—even after internalization by cells [75]—other formulations have demonstrated deleterious effects by producing reactive oxygen species, dissolving into toxic ions (e.g., Ag^+), altering protein folding, inducing DNA damage, or causing membrane thinning and leakage. In some cases, nanomaterials may accumulate in key organs such as liver, spleen or kidney, causing cytotoxicity at otherwise benign doses. These topics have been widely studied and reviewed elsewhere [13, 76, 77].

1D nanomaterials present unique a host of challenges and as a consequence many are more toxic (e.g., exhibit lower LD_{50}) than their isotropic or low aspect-ratio counterparts. Some of these issues relate to the manner in which a cell engulfs—or attempts to engulf—the nanomaterial through endocytic pathways. Typically, nanomaterials are internalized after recruiting receptors that cause the membrane to wrap around the particle; very large particles cannot recruit sufficient receptors to overcome competing elastic forces exerted by the membrane, and so are not internalized. This feedback mechanism fails in the case of 1D nanomaterials, which are believed to enter the cell via a "tip entry" mechanism that prevents the cell from sensing the

length of the nanomaterial. If the nanomaterial is too long for successful internalization and packaging into endosomes, then endocytosis is incomplete and an immune response may be triggered [78]. Such was the case with both TiO_2 [79] and CeO_2 [80] NWs which activated the NALP3 inflammasome, triggering release of proinflammatory mediators IL-1β and increasing likelihood of cell death. In both cases, the phenomena were dependent on the length of the nanomaterial, as short aspect-ratio particles did not demonstrate similar toxicity. In particular, CeO_2 NWs were more likely than shorter nanomaterials to aggregate into bundles that could rupture the lysosome, thereby triggering injurious responses [80]. Similar phenomena were also observed with Ni NWs, which upon exposure to human fibroblasts were apparently localized within lysosomes but altered the size of the endoplasmic reticulum and increased likelihood of cell death [81]. CNT bundles have been reported to exhibit some asbestos-like qualities, causing granulomatous inflammation in the mesothelium *in vivo*; this phenomenon however was confined to bundles that were longer than the length that a macrophage could fully enclose, causing frustrated phagocytosis and a chronic release of proinflammatory cytokines [82].

Also in a matter analogous to asbestos, airborne nanomaterials may accumulate in the lungs resulting in pulmonary toxicity. Intrathecally administered SiNWs induced injury in a rat model, with the longest NWs (15 μm) causing greatest injury as quantified by production of lactate dehydrogenase (LDH), albumin, and proinflammatory cytokines. Inflammation however resolved over time, with approximately 70% of SiNWs cleared by 28 days with most localized within macrophages [83]. Silver NWs, however, appeared to induce chronic effects, including granuloma and foreign body Langerhans cell responses to long (20 μm) and short NWs (2 μm), respectively. Long NWs also exhibited evidence of frustrated phagocytosis [84].

While the mechanisms leading to nanoparticle toxicity warrant careful study, it should be emphasized that rational control over the geometry, composition and surface chemistry of nanomaterials has been shown mitigate or eliminate the deleterious effects described here. Moreover, nanomaterials that are immobilized—e.g., on a planar substrate or within a polymer matrix, is the case with many of the systems reviewed here—are also less likely to induce toxicity since they interface with a relatively small number of cells; studies of silver [85], gold [86] and silicon NWs [87] in immobilized configurations all exhibited little or no cytotoxicity. Ultimately, nanomaterials and nanoelectronic systems will need to be evaluated on a case-by-case basis, analogous to other biomaterials and drug delivery systems [88], to determine their potential for clinical translation.

3 Nanocomposites in tissue engineering

The nanocomposite nature of the ECM plays a key role in morphogenesis and tissue function. Recent studies in tissue engineering have focused on these cues, and how they could be recapitulated in natural or synthetic scaffolds to promote cellular adhesion, spreading and proliferation; to transduce forces; or to create the appropriate electrical microenvironment. Numerous studies have described approaches involving rationally-designed polymers or proteins, which have been reviewed in detail elsewhere [3]. 1D nanomaterials offer a complementary approach to tissue engineering, since in addition to the unique cellular interactions described in the previous section, they can introduce anisotropy that mimics native tissue, present biochemical cues or modulate the mechanical properties of the construct.

3.1 Cardiac tissue engineering

Cardiac tissue engineering represents one area that is especially amenable to nanocomposite scaffolds with conductive 1D components, since cardiac tissue is both anisotropic and conductive. It is also an area of substantial clinical relevance, as heart failure is a leading cause of death worldwide; many patients who suffer from myocardial infarction lose a substantial portion of their myocardium to scar tissue, which disrupts activation pathways and normal heart function. Injectable formulations containing hydrogels and stem cells have been developed to address this issue, and represent one route toward repairing scar tissue [89]. Another route involves the use of cardiac patches—thin constructs of engineered tissues that

can be grafted onto the surface of the heart to restore electrical function. While cardiac patches have shown significant promise, they frequently induce arrhythmias by not adequately integrating with the host tissue. These problems arise in part because materials frequently used in cardiac tissue engineering—proteins, polysaccharides, synthetic polymers—are nonconductive, and therefore disrupt electric field distributions and limit cell–cell interactions. Conductive nanomaterials have been investigated as a means to modulate the conductivity of these patches.

3.1.1 *Nanocomposites for functional cardiac tissues*

The first demonstration of 1D nanomaterials in tissue engineering was achieved with nanocomposite scaffolds composed of AuNWs embedded within the walls of sponge-like, lyophilized alginate scaffolds [86]. While lyophilized alginate scaffolds had been widely explored as cardiac tissue scaffolds because of their amenable chemical and mechanical properties [90], cardiac cells tended to form isolated clusters within the scaffold pores, which would beat asynchronously (Fig. 3(a)). The authors hypothesized that AuNWs would enable electrical and mechanical synchrony by forming conductive bridges across the walls of those scaffolds (Fig. 3(b)). Conducting probe atomic force microscopy (AFM) measurements demonstrated as such—that is, that topographic features arising from the embedded AuNWs were correlated with localized conductance spikes associated with currents flowing across the otherwise insulating film. Cardiac cells dissociated from neonatal rat ventricles were seeded into those scaffolds and cultured for up to 8 days *in vitro* (DIV). Significantly, haematoxylin and eosin (H&E) staining revealed thick, intact and better-aligned tissues compared with tissues cultured in pristine scaffolds. Immunostaining for troponin I, which is involved in muscle calcium binding and contraction, showed strong fluorescence in cells located in the nanocomposite, but not pristine scaffolds on 8 DIV. Western blot analysis also showed a significantly higher expression on 3 and 8 DIV of α-sarcomeric actinin (α-SA) and connexin-43 (Cx-43), which are associated with contractile function and electrical/mechanical cell–cell coupling, respectively (Fig. 3(c)). To assess potential functional differences, the authors also performed Ca^{2+} transient propagation studies on tissues after 8 DIV. They found that within the pristine scaffolds, tissue activity was localized to the stimulation site, with negligible propagation to cells in adjacent pores. In contrast, tissue cultured in the nanocomposite scaffolds demonstrated synchrony across five different

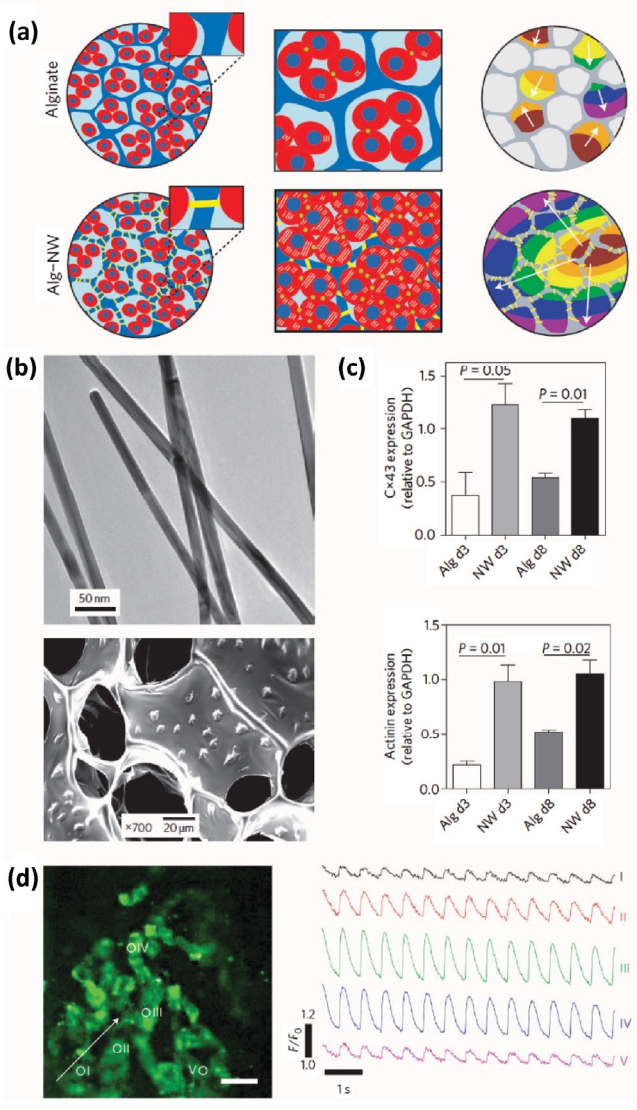

Figure 3 3D nanowired tissues. (a) Schematic overview of 3D engineered cardiac tissues representing (top) isolated clusters in pristine alginate scaffolds and (bottom) mechanical and electrical synchrony in nanowired constructs. (b) (top) TEM of AuNWs and (bottom) SEM of AuNWs embedded within the walls of alginate scaffolds. (c) Quantification of (top) Cx-43 and (bottom) sarcomeric actinin by Western blot in pristine (Alg) or nanowired (NW) scaffolds at day 3 (d3) or 8 (d8). (d) Synchronized calcium transients in nanowired constructs assessed at (left, white circles) specific points with (right) corresponding time course. Adapted with permission from Ref. [86], © Nature Publishing Group 2011.

measurement sites, and over a distance of at least 2 mm (Fig. 3(d)) [86].

The phenomena just described are generalizable to nanomaterials of differing aspect ratios and composition (viz. Au nanospheres [91], Au nanorods [92, 93], CNTs [94], and SiNWs [95, 96]) and also to other types of polymer scaffolds including cast or 3D printed hydrogels, or to cardiac spheroids that did not include any scaffold at all [95, 96] (see next section); numerous groups have explored the mechanisms underlying these unexpectedly broad findings. While nanomaterials appeared to enhance Cx-43 expression in nearly every study, commensurate enhancements in Ca^{2+} signaling alone could not account for improved tissue function; in fact, CNTs maintained electrical activity in cardiac tissues whose Ca^{2+} signaling was inhibited by heptanol, suggesting that they induced cell–cell coupling by some other pathway [94]. Several groups found instead that nanomaterials or nanocomposites enhanced cardiac tissue function by redistributing electric fields, whether endogenous or externally applied. Their conclusion is somewhat supported by theoretical studies suggesting that conductive substrates could form bridges between adjacent cell groups, thereby transferring signals from active to passive domains. However, the authors also concluded that nanomaterial bridges would need to form an extremely tight seal ($> 10^{13}$ Ω/sqr) with the cell membrane which is unlikely for planar substrates but might be achievable with nanomaterials given the tight junctions described in Section 2.2; alternatively nanotopographic cues may enhance tissue organization or recruit ion channels [97]. Given these remaining ambiguities, further studies are warranted.

3.1.2 *NWs in cardiac spheroids*

SiNWs enhanced the function of cardiac spheroids, which presented tissue-like microenvironments without the need for scaffolds. In that work, the NWs were heavily doped to impart high conductivity (150–500 μS/μm) so that they could form a conductive network in the relatively less-conductive culture medium (ca. 1.75 μS/μm) and myocardium (ca. 0.1 μS/μm). As was the case with the nanocomposite constructs described previously, nanowired spheroids demonstrated more synchronous and larger amplitude contraction compared to their pristine counterparts. Substantially, the authors demonstrated that the improvements could be attributed to Cx-43, whose expression at 7 DIV was increased two-fold by NWs; and to α-SA, whose expression at the same time point was increased by application of an exogenous electric field stimulus (Fig. 4) [95].

These findings suggested that the endogenous effects of the NWs coupled with the exogenous electric field could synergistically improve cardiac spheroid functions by enhancing both Cx-43 and α-SA expression. The authors investigated this synergy by applying stimuli to mature spheroids, both nanowired and pristine, for 9 DIV. They found that the combination of those two factors not only improved cell junction formation, but also increased contractile properties and reduced endogenous beat rate, which implied an increased cardiomyocyte developmental age [96].

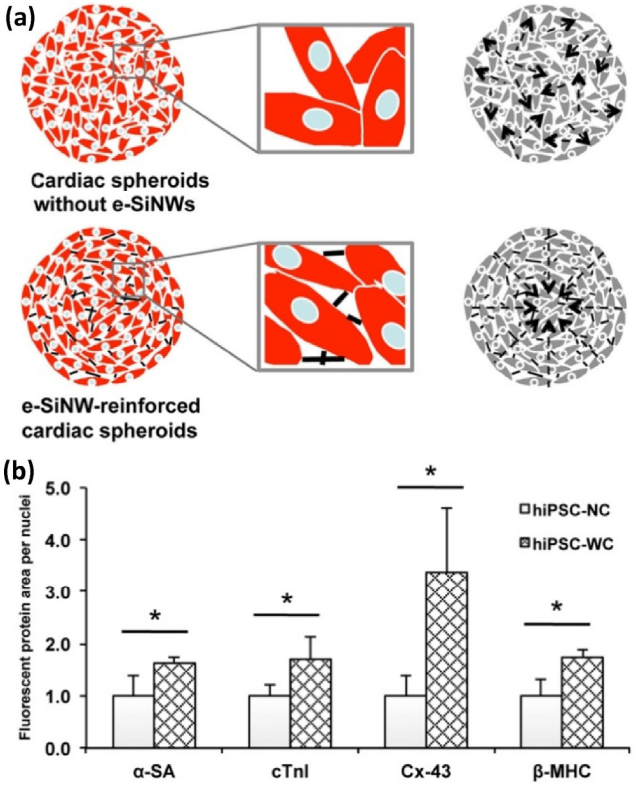

Figure 4 Nanowired cardiac spheroids. (a) Schematic overview of cardiac spheroids forming (top) electrically isolated small beating clusters without SiNWs or (bottom) synchronized contractions with SiNWs. (b) Protein expression analysis on spheroids with (WC) or without (NC) NWs (*$p < 0.05$). Adapted with permission from Ref. [95], © American Chemical Society 2015; Ref. [96], © American Chemical Society 2016.

3.2 Nerve tissue engineering

Because neural tissue function relies highly on proper electrical signaling, it is no surprise that nanomaterials that support or enhance electrical signaling can have beneficial effects on engineered tissue. In fact, groups have shown that incorporating carbon nanofibers (CNFs) [98], CNTs [60], silicon NWs [59], and other electrically conductive nanomaterials could enhance functioning of engineered neural tissue. For example, single-walled carbon nanotubes (SWCNTs), incorporated within collagen-matrigel composite hydrogels were shown to enhance neurite outgrowth in a non-dose dependent manner [99]. Similar effects were observed with organotypic spinal cord slices cultured on multiwalled carbon nanotube (MWCNT) mats, which showed an increased number and length of neurite outgrowths and increased expression of the cytoskeletal components F-actin and βIII-tubulin, and also appeared to improve synchronization between nerve networks and synaptic boutons [100].

Complementary to applications directly regarding the brain, nanomaterials have also been utilized to guide peripheral nerve growth. Nerve guidance conduits (NGCs) composed of polycaprolactone (PCL) and single-layered graphene (SG) or multi-layered graphene (MG) doped with polydopamine (PDA) and arginylglycylaspartic acid (RGD) were shown to enhance nerve regrowth. In addition to promoting axonal regrowth and remyelination following peripheral nerve injury, this scaffold was able to improve neural expression *in vitro* and *in vivo* [101]. The reported increase in both GFAP and Tuj1 expression was particularly exciting, because it suggested that this scaffold could induce differentiation into both neural and astrocytic lineages. In addition to the enhanced expression of GFAP and Tuj1, proliferative markers (Brdu and Ki67), cell attachment markers (N-cadherin and vinculin), and neurotrophic factors (BDNF, NGF, GDNF, and CNTF) were enhanced significantly in nearly all CNT-containing groups [101].

While utilization of nanomaterials for neural tissue engineering is just really beginning to be explored, it is nonetheless an exciting prospect. Because different nanomaterials have the capacity to direct NSC differentiation, their use in neural tissue engineering will likely lead to the development of more robust brain models that include multiple cell types oriented in a manner to more accurately replicate native brain structure and function.

3.3 Anisotropy and specialized structures

With the plethora of variables involved with developing nanomaterials for use in tissue engineering, anisotropy is an essential yet often neglected property. Because many biological tissues (muscle, nerve, cornea, cartilage, bone, etc.) display anisotropy in both structure and physicochemical properties, it is especially important to consider the role of anisotropy of nanomaterials used in tissue engineering constructs [102–107]. By imbuing tissue engineering scaffolds with anisotropic properties (e.g., electrical anisotropy via aligned CNTs [108]), one can direct tissue-specific morphology changes, differentiation, and adhesion to more accurately recapitulate the effect of native ECM and tissue function. In fact, many groups have recently taken advantage of using anisotropic scaffolds for engineered cardiac tissue [102, 107] and skeletal-muscle tissue [103–106].

It is important to note that anisotropy can be morphological, chemical, or a mixture of the two. For example, nanorods or nanowires can be considered morphologically anisotropic—they possess anisotropic rod-shaped structures but are chemically homogeneous. Janus particles—which are generally spherical nanoparticles with each hemisphere composed of a different chemical composition—are considered chemically anisotropic. Similarly, a nanowire doped at each end with a compound that differs from the bulk material of the nanowire could be considered both morphologically and chemically anisotropic [109].

While anisotropy has traditionally been studied more with respect to bone, cardiac, and muscle tissue, many groups are working to extend the use of anisotropic scaffolds to other domains. Rose and colleagues recently developed an injectable anisotropic hydrogel doped with superparamagnetic iron oxide nanoparticles (SPIONS) that aligned upon application of an external magnetic field and became fixed in place following gelation. This anisotropic matrix was able to align both fibroblasts and cells from dorsal

root ganglia (DRG) along the direction of the applied magnetic field. While this approach has yet to be applied *in vivo*, it may hold the potential to develop new therapies for spinal cord and peripheral nerve injuries [106].

The utility of anisotropy in tissue engineering scaffolds is widely dependent on the target tissue—many cell types (e.g. liver, pancreas, or kidney) are polarized (containing basal, lateral, and apical surfaces, which contact the ECM, neighboring cells, and the lumen, respectively) and in those cases, the anisotropy of the scaffold may not be nearly as important as the general location of the scaffold (i.e. the scaffold should be exposed to the basal surface, as its purpose is to recapitulate native ECM) [3]. In any case, it is difficult to say with certainty whether a certain tissue could react favorably by inducing anisotropy into scaffolds, regardless of native tissue structure. It could be that even isotropic tissues could benefit from being grown on an anisotropic scaffold, or that anisotropic scaffolds could be used to induce novel behavior when used with isotropic tissues. As anisotropy becomes increasingly considered with respect to tissue engineering applications, we will continue to better understand its effects, and thus increase our ability to develop more robust, sophisticated tissue engineered scaffolds.

4 Nanoelectronics

Semiconductor nanomaterials elucidated as nanoelectronic devices have opened entirely new avenues for achieving two-way interfaces with cells and tissues with high spatial-and temporal resolution. These interfaces are complementary to conventional techniques such as patch-clamp electrodes, multielectrode arrays (MEAs), and optical dyes, but offer distinct advantages as well. For example, patch-clamp electrodes are difficult to multiplex and cannot be readily integrated within tissues. MEAs cannot be readily miniaturized to subcellular scales because of factors such as Johnson-Nyquist noise, which scales inversely with size [110, 111]. Finally, optical dyes require sophisticated instrumentation and may be susceptible to toxicity and photobleaching effects.

Nanoelectronic devices may be achieved from nanomaterial building blocks through the bottom-up assembly paradigm: First, nanomaterials are synthesized with rationally-controlled geometry and chemical composition, then they are assembled onto the appropriate substrate and addressed with interconnects. This paradigm is especially apropos for biological interfaces since nanomaterial synthesis typically takes place at high temperatures and low pressures and involves caustic precursors that are not compatible with biological materials. Once synthesized, however, nanomaterials may be incorporated within biological substrates at a wide range of length scales—ranging from subcellular to tissue-scale—while enabling independent control over the chemical and mechanical properties of the substrate. Assembly techniques have been developed to achieve ensembles in both two-dimensional (2D) and 3D, and have been reviewed elsewhere [112].

4.1 Nanowire field-effect transistors (NW-FETs) for cell and tissue interfaces

Semiconductor NW-FETs represent one class of nanoelectronic devices that has shown extraordinary potential as biological sensors [113]. They are analogous in many ways to conventional metal oxide semiconductor field effect transistors (MOSFETs): source (S) and drain (D) electrodes may be deposited by conventional lithography techniques, the NW channel may be impregnated with n- or p-type dopants, and its conductance changes in response to variations in the surface charge or local potential. Within the context of biological systems, variations in this gate voltage may be achieved by changes in chemical environment (e.g. pH) or by binding of a biological species (e.g. protein, virus, nucleic acid) to the surface of a NW (Figs. 5(a) and 5(b)). More recently, NW-FETs have been used to measure intra- or extracellular potentials from electrically active cells such as neurons or cardiomyocytes (Figs. 5(d) and 5(e)).

4.1.1 Extracellular interfaces at the cellular level

NW-FETs assembled onto planar substrates have enabled noninvasive studies of cellular signaling by measuring extracellular spikes (Fig. 5(c)(i)). The seminal study in this area involved interfaces with rat cortical neurons, where neurite growth was guided over

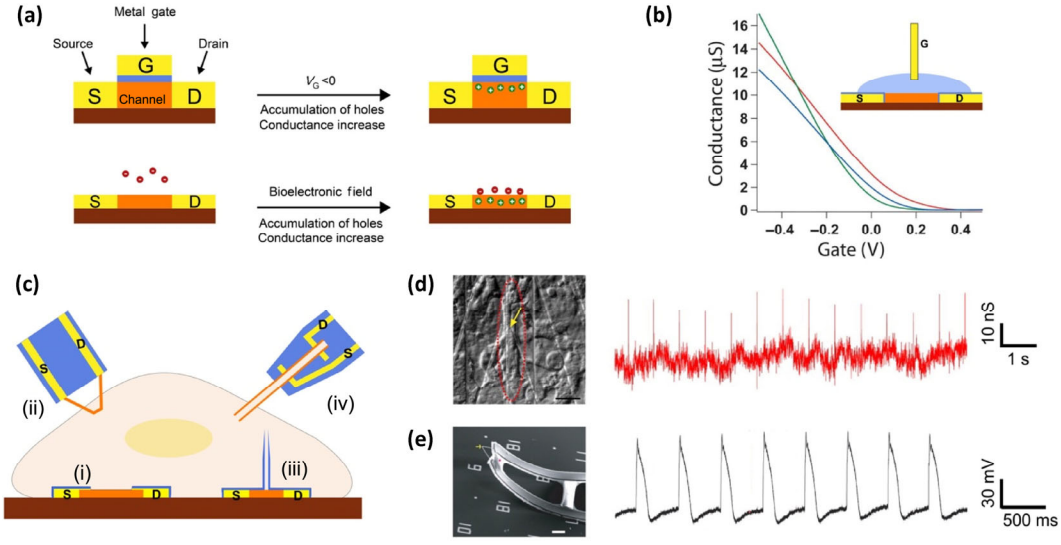

Figure 5 NW-FET function and cellular interfaces. (a) (top) Schematic of a p-type planar FET device, where S, D, and G correspond to source, drain and gate electrodes, respectively. (bottom) Schematic of NW-FET equivalent, where channel is gated by a bioelectric field. (b) Conductance vs. water gate voltage for three NW-FET devices; inset, scheme representing experimental setup, which includes (orange) NW, (yellow/blue) passivated contact electrodes, (light blue) electrolyte solution, and (yellow) Ag/AgCl reference/gate electrode. (c) Schematic of NW-FET configurations: (i) planar NW-FET, (ii) kinked NW-FET, (iii) BIT-FET, and (iv) ANTT. (d) (left) Optical image of planar NW-FET interfaced with cardiomyocyte monolayer and (right) corresponding extracellular signal. Scale bar, 20 μm. (e) (left) SEM of kinked NW-FET probe and (right) corresponding intracellular signal from cardiomyocyte. Scale bar, 5 μm. Adapted with permission from Refs. [114], © American Chemical Society 2009; Ref. [115], © American Chemical Society 2009; Ref. [116], © American Association for the Advancement of Science 2010.

individual NW-FETs, which could record multiplexed extracellular signals at subcellular resolution [117]. In this study, p-type NWs recorded positive conductance spikes (negative potential spikes) that were correlated in time with the intracellular AP. NW-FETs interfaced with primary cardiomyocytes [115], HL-1 cells [118], and smooth muscle cells [119] also recorded extracellular signals, although those signals were typically biphasic (Fig. 5(d)).

Variations in the magnitude and shape of the extracellular potential are a result of the complex interplay between the geometry of the cell, spacing of the junction between cell and substrate (cleft), and ion channel expression. Extracellular NW-FETs measure voltage fluctuations induced by ionic flows through the cleft; direct measurements of the intracellular potential or of the surface charge of the membrane are precluded due to Debye screening effects. Equivalent circuit models and accompanying mathematical analyses have been developed to model ion flows, and hence the relationship between intra- and extracellular potentials, for MEAs [120–122], although these models could be extended to planar NW-FET measurements with some modifications. Notably, the shape and magnitude of the extracellular signal is critically dependent on the distribution of Na^+, K^+ and Ca^{2+} channels, which may be altered by interactions with the substrate, and, as alluded to in previous sections, by the nanomaterial interface. Additionally, the distance of the cleft, 10–100 nm on planar substrates [37, 123], plays a role since it affects the seal resistance; studies on NW-FET/cardiomyocyte interfaces showed a commensurate increase in signal magnitude as the cleft spacing was reduced by mechanical manipulation of the cell monolayer [115]. A direct comparison between planar electrodes and NW-FETs interfaced with HL-1 cells demonstrated that the NW-FETs could record signals with larger magnitude and higher signal-to-noise, presumably because of these unique nanoscale interactions [118].

While FETs composed of NWs or other 1D building blocks exhibit distinct advantages over their microscale counterparts, they typically do not offer true "point-like" contacts since signals are averaged over the

entire length of the channel, typically on the order of 1–2 μm, thereby limiting the spatial and temporal resolution of the recordings. To address this limitation, short-channel $n^{++}/n/n^{++}$ or $n^{++}/i/n^{++}$ NW-FETs were developed by modulating the dopant concentration during the growth process [124]. The degenerately-doped n^{++} regions functioned as conductive conduits to the n-type or intrinsic channel, whose length could be varied between 40 and 160 nm. Signals recorded from those short-channel devices exhibited peak-to-peak widths of 450–540 μs, substantially smaller than the 750–850 μs widths reported for devices with micrometer-scale channels. They were of sufficiently high resolution to resolve timing shifts from devices with separations less than 2 μm, enabling studies of signal propagation both within a single cell and across cell–cell junctions [124].

4.1.2 *Intracellular interfaces*

As should be evident from the previous section, a complete picture of the intracellular potential, particularly subthreshold depolarization or hyper-polarization, cannot be readily derived from extracellular measurements alone. One distinct advantage of NW-FETs—and one that substantially differentiates them from their microscale counterparts—is that they can be elucidated as free-standing structures that can penetrate the cell membrane, thereby enabling stable access to the cytosol. Unlike patch clamp pipettes, these NW-FETs can be multiplexed, and minimally perturb the membrane, potentially enabling long-term studies.

NW-FETs with kinked NW building blocks represent one such class of intracellular probes. In this configuration, each arm was connected to an S or D electrode while the kinked region—forming a 60° angle—could record intracellular potential via a local point-like gate encoded by $n^{++}/n/n^{++}$ or p/n modulation doping (Fig. 5(c)(ii)). In a seminal study, kinked NW-FETs were designed to protrude from a planar substrate because of bilayer strain, and their penetration into the cytosol of HL-1 or primary cardiomyocyte monolayers was facilitated with a lipid bilayer coating [116]. Those devices could clearly measure the ca. –50 mV membrane resting potential. Upon penetration into a firing cardiomyocyte, a clear transition was observed between extracellular recordings—similar to those described in the previous section—and intracellular recordings. Significantly, the intracellular measurements revealed characteristic features of fast cardiac action potentials, demonstrating the ability of NW-FETs to collect electrophysiological data with similar fidelity to patch clamp pipettes (Fig. 5(e)) [116]. While the devices in this initial study were confined to fixed positions on planar substrates, subsequent elaborations involved kinked NW-FETs that could be moved in three dimensions with a standard three-axis micromanipulator, enabling targeted recording from specific cells or subcellular structures [64], or, using multiplexed devices, from two spatially-distinct regions within the same cell [125].

Intracellular probes have also been achieved using nanotubes, which were fabricated by deposition of silicon or silicon oxide shells onto sacrificial germanium NW templates. Branched-nanotube intracellular field-effect transistors (BIT-FETs) consisted of a silicon oxide nanotube grated onto a silicon NW backbone, which functioned as the channel of the FET (Fig. 5(c)(iii)). In this configuration, the tip of the germanium template could be tapered prior to oxide deposition, enabling BIT-FETs with sub-10-nm diameter [126]. Active silicon nanotube transistors (ANTTs) were also fabricated by defining S and D electrodes directly onto the nanotube, which itself acted as the channel, while SU-8 passivation on the electrodes effectively shielded the device from extracellular contributions (Fig. 5(c)(iv)) [127]. In either case, the nanotube could readily penetrate a cell membrane, causing the interior of the nanotube to form an electronic junction with the cytosol.

4.1.3 *Multiplexed interfaces with ex vivo or engineered tissues*

A key advantage of the bottom-up approach is that devices can be assembled on a wide range of length scales ranging from subcellular to tissue-scale, as well as a variety of transparent, flexible, and/or conformal substrates. These capabilities have enabled studies of signal propagation from *ex vivo* tissue preparations. Multiplexed NW-FET device arrays arranged on flexible, polyimide substrates enabled measurements of field potential propagation vectors across the surface of spontaneously-beating myocardium (Fig. 6(a))

[114]. NW-FET device arrays also enabled network connectivity analysis within acute brain slices (Fig. 6(b)), including identification of features associated with presynaptic firing and postsynaptic depolarization as well as mapping of heterogeneous connectivity throughout the olfactory cortex [128].

NW-FETs were achieved within the void spaces of flexible, macroporous substrates that could be embedded within engineered tissues to achieve localized electrical or chemical sensing [129]. These nanoelectronic scaffolds (nanoES) were designed with > 99% void space, and so could be readily integrated with ECM typically used to support 3D tissue culture, including natural or synthetic hydrogel or fiber constructs (Fig. 6(c)). The hybrids supported 3D culture of both rat cortical neurons and cardiomyocytes, and achieved multiplexed electrophysiological recordings at a level of four devices. Because of their flexibility, nanoES could be wrapped into cylindrical geometries without affecting device performance to achieve vascular-like constructs that could achieve pH measurements from fluid flowing through the lumen. Scaffolds with up to 64 devices were folded into multilayer structures to achieve 4 × 16 device arrays that recorded 3D isochronal maps from cardiac tissue (Fig. 6(d)) [87]. Significantly, nanoES recorded maps for at least 8 days after cell seeding, showing an increase in signal yield and amplitude commensurate with tissue maturation and formation of synchronous 3D networks.

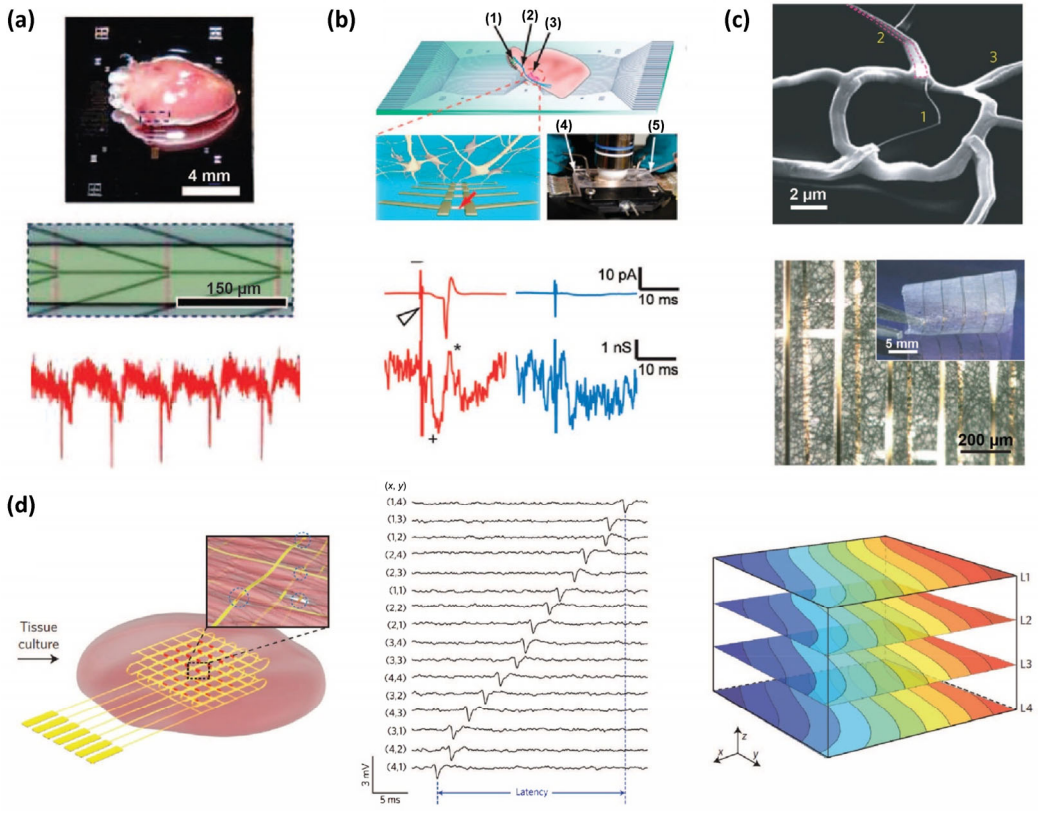

Figure 6 NW-FETs at the tissue level. (a) NW–heart interface. (top) Optical photograph of heart, (center) photograph of array of three-element NW-FET device array, and (bottom) representative conductance traces of NW-FETs from heart. (b) NW–brain interface. (top) Schematic of NW-FET array interfaced with pyramidal cell layer of brain slice and (bottom) conductance recording from a NW-FET (lower traces) and patch clamp (upper traces) from tissue stimulated with strong (red) or weak (blue) currents. (c) NW interface with synthetic tissue. (top) SEM image highlighting (1) a kinked-NW-FET, (2) SU-8 scaffold and (3) metallic interconnect; and (bottom) bright-field optical micrograph of the folded scaffold. (d) (left) Schematic of nanoelectronic–cardiac tissue with folded nanoelectronic scaffold, (center) simultaneous traces recorded from 16 sensors in one layer of the nanoelectronic–cardiac tissue and (right) 3D isochronal map of latency throughout the construct. Adapted with permission from Refs. [87], © Nature Publishing Group 2016; Ref. [114], © American Chemical Society 2009; Ref. [128], © National Academy of Sciences 2010; Ref. [129], © Nature Publishing Group 2012.

4.1.4 *Injectable electronics*

Nanoelectronic systems have been integrated within syringe-injectable systems that could be introduced into spatially-confined spaces, including the cranial cavity of living animals, in a minimally invasive manner. These meshes were centimeter-scale, but exhibited suitable mechanical properties such that they could be folded and loaded into, and then partially ejected from, a 100 μm diameter glass or metal syringe [130]. Post-injection, the meshes either expanded to fill the cavity, or, in the case of tissue, formed a conformal and minimally-disruptive interface with the surrounding cells. Many types of mesh electronics have been developed, including those that supported microscale electrodes, piezoresistive strain sensors, and NW-FETs. In all cases, the I/O pads on the free end of the mesh substrate were connected to external electronics either through an anisotropic conductive film, conductive printed ink [131], or a zero-insertion force (ZIF) connector [132], enabling multiplexed device measurements with high yield.

Mesh electronics were injected into the cranial cavities of live, anesthetized rats by stereotaxic injection. Targeted delivery of the mesh to a specific region of the tissue was achieved by incorporating a controlled injection setup consisting of a programmable syringe pump that could inject the mesh with a fixed volumetric flow rate, coupled with a motorized stage that could withdraw the syringe at constant velocity set to match the ejection rate from the needle. This technique achieved device placement with up to 20 μm resolution, even within opaque tissues [131].

In vivo, mesh electronics offered substantial advantages over other state-of-the-art thin-film brain probes. Because of their relatively small size, mesh electronics were implanted though a far less invasive surgical procedure, via an opening in the skull on the scale of hundreds of microns. Moreover, after implantation, conventional polymer or metallic probes led to an accumulation of astrocytes and microglia, presumably because of mechanical mismatches with the surrounding tissue. Mesh electronics offered a combination of structural and mechanical features that minimized immune response; they readily allowed for interpenetration of axons through their pores and exhibited a relatively low bending stiffness of ca. 0.1 nN·m, on the order of that of a brain tissue slice. Significantly, mesh electronics showed a uniform distribution of astrocytes, microglia and neurons between weeks 2–12 *in vivo* [133], demonstrating their ability to interface with brain tissue noninvasively. Meshes with metallic recording elements enabled stable recordings from the hippocampus and somatosensory cortex of live mice at single-neuron resolution [134], from up to 128 channels simultaneously for at least 8 months [135].

4.1.5 *Longevity*

Studies of NW-FETs have generally been confined to a timeframe of days to weeks. They may degrade over longer periods since the native SiO_2 surface passivation layer, while stable in the dry state, is subject to hydrolysis in aqueous solutions [136]. This property of silicon has in fact been exploited to achieve bioresorbable electronics [137, 138]. In other cases, long term nanoelectronic interfaces may be desirable, particularly for clinical applications relating regenerative medicine or diagnostics. To address NW-FET stability for these applications, the NW channel was passivated with a 10 nm thick AlO_2 or HfO_2/AlO_2 nanolaminated shell, both of which are high-κ dielectrics that did not substantially affect the initial performance (e.g. conductance, transconductance) of the devices. They were deposited via alternating layer deposition, which created conformal, pinhole-free layers that exhibited excellent stability in physiological media. AlO_2 or HfO_2/AlO_2 shells extended the lifetime of the devices for up to 100 days or 1 year, respectively [139].

4.2 Passive nanowire electrodes

Vertical NWs connected to planar metallic electrodes have been used as to passively measure electric fields. While these structures have been used to measure extracellular fields in a manner analogous to MEAs, they offer the added advantage that they may enter the cytosol and record intracellular signals following membrane poration or other techniques as described in Section 2.5 (Fig. 7) [63]. Pt NW arrays recorded stable intracellular signals from HL-1 cells [67] and human induced pluripotent stem cell (hiPSC)-derived cardiomyocytes [140] for about 10 min following electroporation. They could distinguish between slow

and fast action potentials, characteristic of pacemaker and non-pacemaker cardiomyocytes, respectively, and could also measure the effects of representative Ca^{2+} or K^+ ion channel blockers [67]. Similar vertical geometries—Si NWs sputter coated with metallic tips—achieved intracellular measurements from cultured neural networks and mapped individual synaptic connections [141]. Dense arrays of vertical Si NWs also allowed for intracellular recordings from hiPSC-derived neurons at 6 weeks *in vitro* [142].

Techniques used to fabricate the devices just described have been combined with nanomaterial synthesis routes to achieve vertical NW arrays with tailored properties.

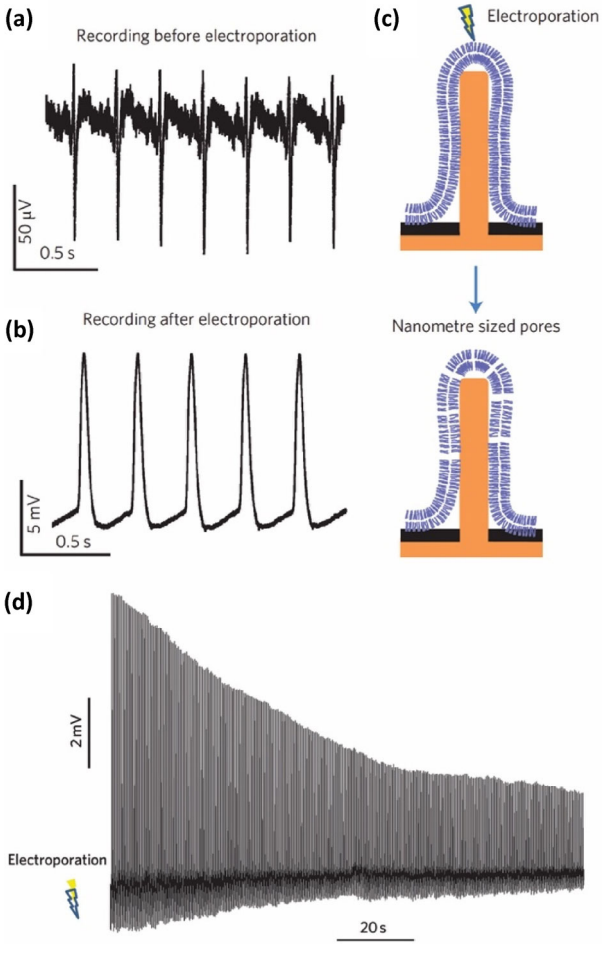

Figure 7 Electrophysiological measurements from vertical NW electrodes. Recorded train of (a) extracellular action potentials, before electroporation and (b) intracellular action potentials, after electroporation. (c) Schematic of electroporation of the cell membrane by a nanopillar electrode. (d) Trace of intracellular action potential decaying over time due to sealing of transient pores in the membrane. Adapted with permission from Ref. [67], © Nature Publishing Group 2012.

For example, plasmonic nanoelectrodes capable of optical poration were achieved by coating polymer NWs with Au shells. Short-pulse laser stimulation (8 ps, 1,064 nm) generated an electromagnetic field localized at the NW tip that was strong enough to mechanically disrupt the membrane. This process caused less damage to the cell and yielded a tighter electrical junction than other poration techniques, which are less spatially selective [66]. The nature of the electrode junction itself was also explored with iridium oxide nanotube electrodes, which formed a tight junction when the cell membrane protruded into the nanotube cavity. These devices enabled intracellular recording for up to an hour, for up to eight consecutive days [68].

NW electrodes have also been used to achieve recordings *in vivo*. Single-crystalline Au NWs attached to insulated tungsten tips were implanted into live rat brains, and recorded signals with single neuron resolution, affording signals with substantially higher spatial and temporal fidelity than could be achieved by conventional tungsten electrodes alone. Neural network mapping was achieved by applying cross-correlation techniques with electrode pairs, enabling identification of brain response to external stimuli or localization of seizure center in an epilepsy model [143].

4.3 Stimulation devices

Electrophysiological recording devices are often used in conjunction with stimulation elements that simulate pacing or synaptic inputs. Conventional stimulation elements consist of macro- or microscale metallic surfaces that inject current into surrounding tissues via capacitive coupling; these simulation elements are large compared to the size of a single cell and may introduce capacitive transients that preclude simultaneous recordings. Advances in nanoscience have addressed these limitations, enabling single-cell stimulation with very small but highly localized currents. For example, vertical NW arrays as described in the previous section have been used to inject currents directly into the cytosol of cultured neurons, enabling network activation at the single-cell level [141].

Stimulation has also been achieved via photocurrents produced by optically active nanomaterials. This principle was demonstrated with thin films containing

HgTe or CdTe quantum dots, which supported neuron culture and could produce sub- or supra-threshold depolarizing currents upon irradiation with laser light [144, 145]. While these studies demonstrated the utility of quantum confined systems in biology, the films themselves were macroscale and therefore modulated ensembles of neurons. Recently, neuromodulation was demonstrated at the single-cell level with free-standing coaxial p-type/intrinsic/n-type (p/i/n) silicon nanowires, in which generated photocurrents when irradiated with a pulsed 532 nm laser source (Fig. 8(a)). These NWs also presented surface-diffused Au clusters, which the authors hypothesized

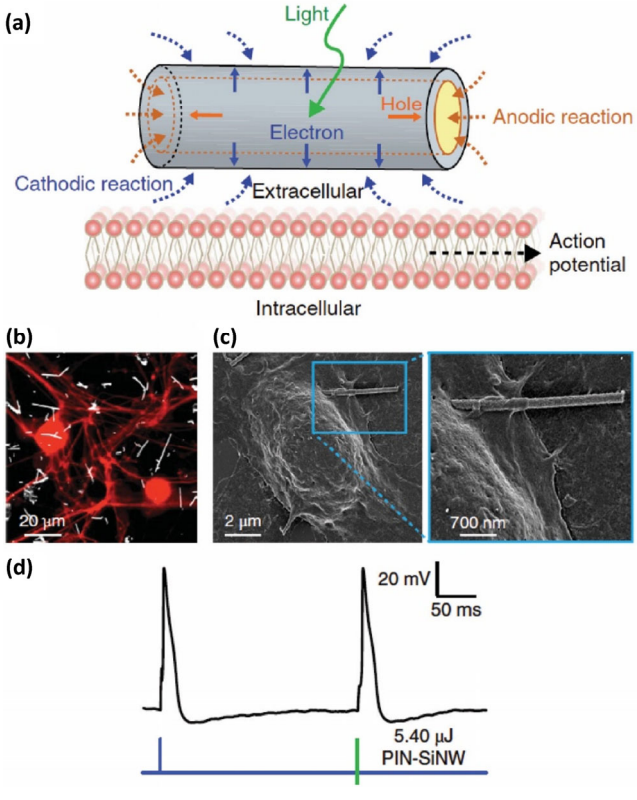

Figure 8 NW stimulation. (a) Schematic of the current produced by a p/i/n SiNW at the neuronal cell membrane upon light stimulation, representing movement of electrons (blue lines) and holes (orange lines) and cathodic (blue dotted lines) and anodic (orange dotted lines) reactions. (b) Confocal microscopy image of stained DRG neurons (red) co-cultured with SiNWs (white). (c) SEM image of a single DRG neuron interacting with a single SiNW (left) and a zoomed in image showing the neuron/SiNW interface (right). (d) Patch-clamp electrophysiology current-clamp trace of membrane voltage with SiNW neuron stimulated by injected current (blue) and a laser pulse (green). Adapted with permission from Ref. [146], © Nature Publishing Group 2018.

accumulated photogenerated electrons and served as sites for a cathodic reaction with electrolyte medium. These NWs were drop-cast onto cultured neurons or DRG and formed tight junctions with the external surface of the cell membranes enabling neuronal stimulation at the single-NW level, with action potentials similar to those achieved with conventional patch clamp pipettes (Figs. 8(b)–8(d)) [146].

5 Modeling for rational nanoparticle design

While nanomaterials have been widely used in and extensively characterized for biological interfacing applications, choosing relevant nanomaterials still largely comes down to guesswork. Because of the great diversity in structural characteristics of nanomaterials and the fact that many are built in-house, empirical physicochemical properties of nanomaterials are typically ill-defined [147]. While molecular dynamics (MD) can effectively model many nanomaterial interactions, they are computationally expensive, and are not currently sophisticated enough to give significant insight into more complex processes such as cytotoxicity [147]. Despite this difficulty, significant strides are being made in developing increasingly sophisticated methods to lower the computational cost of these simulations [148] and many of these methods are sufficient to describe certain properties exhibited by nanomaterials, such as contact angle probability distributions for wetting at the nanoscale [149] and receptor-mediated endocytosis of nanoparticles [150].

Another more recent computational approach to the modeling of nanomaterials involves a technique called quantitative structure-activity relationship (QSAR) modeling. Incidentally, QSAR has been around since the 1960s—it was developed by chemist Corwin Hansch to understand how 3D chemical structure impacts activity in plant growth regulators [151]. QSAR involves using a collection of "chemical descriptors" such as molecular formula, surface area, ligand type, etc. to extrapolate possible biological (or other) activities through the application of statistical and/or machine learning-type algorithms [151, 152] (Fig. 9). While QSAR has been widely used in drug discovery

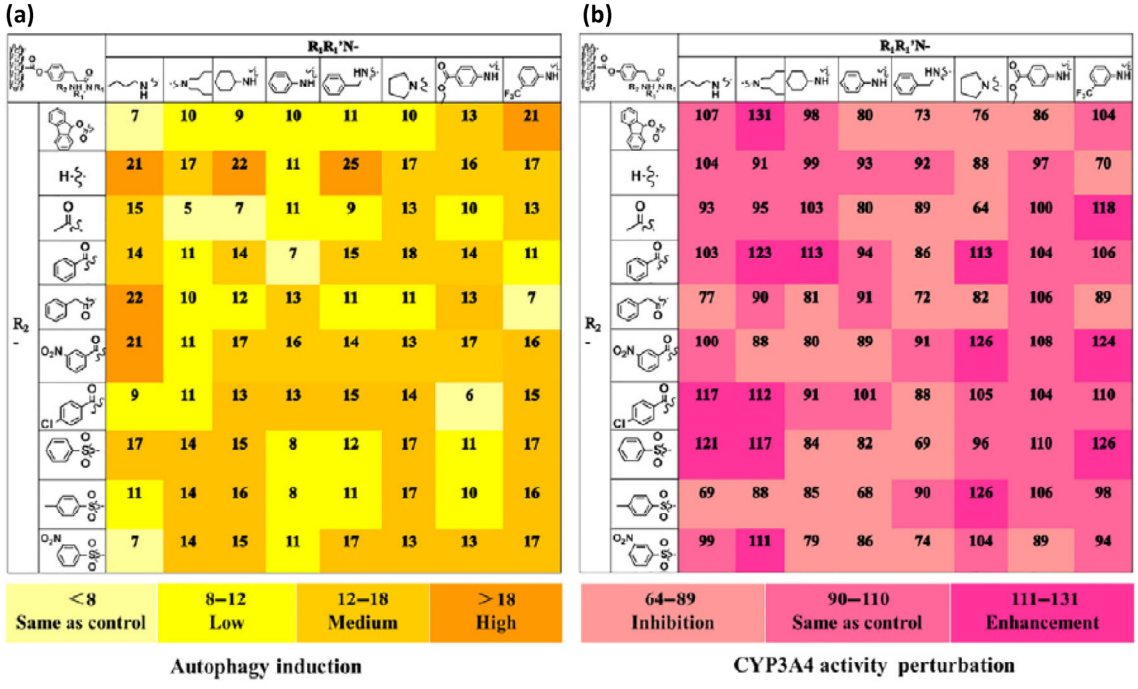

Figure 9 Nanomaterial modeling by nano-QSAR. Heat-maps of (a) autophagy induction, and (b) CYP3A4 perturbation, by a library of MWCNTs, demonstrating the utility of a nano-QSAR approach to nanomaterial design. Adapted with permission from Refs. [153], © Elsevier 2017; Ref. [154], © American Chemical Society 2014; Ref. [155], © John Wiley & Sons 2016.

and computational toxicology, it has scarcely been used to model nanomaterials due to the lack of appropriate descriptors [147, 151]. However, in the past decade or so, the use of QSAR to describe nanomaterials (often coined "nano-QSAR") has steadily increased due to the increasing ubiquity of nanomaterials and the need to adequate characterize them [151, 156]. Because QSAR requires the use of numerous chemical descriptors, the development and availability of effective descriptor libraries for nanomaterials is essential [153]. Due to the complexities of nanomaterials compared to small molecules (e.g. nanomaterials exist not as discrete particles but as distributions), generation of specific molecular "nano-descriptors" (which can be developed both experimentally and computationally) is exceedingly difficult [153]. Although much work has gone into developing effective nano-descriptors, their difficulty of development still constitutes a large barrier to the use of nano-QSAR. Additionally, due to experimental variability between labs, experimentally developed nano-descriptors will often vary greatly from lab to lab [147, 153, 156]. Nano-QSAR models are increasingly able to predict complex phenomena such as MWCNT cytotoxicity in human lung cells [157], metal oxide nanoparticle inhibition of zebrafish hatching enzyme (ZHE1) [156], cellular uptake of a variety of gold nanoparticles in human cells [147], and effects of surface-modified MWCNTs on cellular autophagy and CYP3A4 liver enzyme function [56, 154].

It should be noted that molecular dynamics simulations and QSAR are not mutually exclusive—molecular dynamics simulations can and will likely be increasingly used to determine chemical descriptors that may be difficult to obtain experimentally. Computationally derived nano-descriptors also have the benefit of being well defined—something that is difficult to achieve for experimentally derived nano-descriptors. In particular, it is likely that the increasing sophistication of molecular dynamics simulations of SAMs [158, 159] will lead to the increased ability to develop nano-descriptors for surface-modified nanoparticles. While nano-QSAR is still in its infancy, the field is likely to become increasingly relevant in the next few decades as new nanomaterials continue to be developed and used.

6 Conclusions and future directions

We have described the role of 1D nanomaterials in biological systems at various levels of complexity by describing their ability to fundamentally modulate cellular activity, to recapitulate the ECM and promote morphogenesis in engineered tissues, and to function as building blocks in active nanoelectronics for monitoring tissue function with unprecedented spatial and temporal resolution. Looking forward, nanomaterials are likely to augment biological systems in increasingly sophisticated modalities, enabling new classes of hybrid tissues with functions that mimic or extend those of their native counterparts. First, advances in 3D bioprinting techniques [160] along with specialized nanocomposite bioink formulations [93] are enabling increasingly sophisticated constructs that exploit the unique nanoscale interactions described here while also recapitulating the heterogeneity of native tissues. Second, new classes of nanomaterials are likely to enable entirely new types of functional bio-interfaces; emerging examples include piezoelectronic elements that can harvest energy [161] or optoelectronic devices [162] that may interface with tissues expressing optically-active ion channels. Finally, new substrates could complement the functionality of these devices, for example by imparting biodegradability [137] or wireless communication capabilities [163]. These examples of rational system design will likely be guided by advances in nanomaterial modeling, possibly using nano-QSAR or other techniques that may enhance our ability to develop novel nanomaterials with rationally defined physicochemical properties for use in tissue engineering and other applications. As these models continue to improve, we will be able to better estimate biological responses to nanomaterial composition, surface modification, and numerous other properties that will potentially allow for faster and more sophisticated nanomaterial design.

It is important to note that advances reviewed here are complementary to many emerging opportunities in tissue engineering. For example, new classes of innervated tissues (e.g., cornea [164] or brain [165]) could enable fundamental studies in neuroscience and quantitative assessments of pain or injury. Functional intestine models have also been developed [166], and are likely to contribute to a growing body of knowledge about the gut-brain axis and role of the microbiome in cognition and homeostasis [167]. Techniques to stimulate the development of neural networks within those systems and to interface with them in a multiplexed, two-way fashion could enable new modalities for probing the state of a tissue, driving its function, and understanding communications pathways.

Acknowledgements

The authors wish to acknowledge: China Research Council Award, No. [2016]3100 to H. T. L.; National Defense Science and Engineering Graduate Fellowship to B. H.; and Tufts Collaborates Award to B. P. T.

References

[1] Timko, B. P.; Whitehead, K.; Gao, W. W.; Kohane, D. S.; Farokhzad, O.; Anderson, D.; Langer, R. Advances in drug delivery. *Annu. Rev. Mater. Res.* **2011**, *41*, 1–20.

[2] Wang, Y. F.; Kohane, D. S. External triggering and triggered targeting strategies for drug delivery. *Nat. Rev. Mater.* **2017**, *2*, 17020.

[3] Dvir, T.; Timko, B. P.; Kohane, D. S.; Langer, R. Nanotechnological strategies for engineering complex tissues. *Nat. Nanotechnol.* **2011**, *6*, 13–22.

[4] Cohen-Karni, T.; Langer, R.; Kohane, D. S. The smartest materials: The future of nanoelectronics in medicine. *ACS Nano* **2012**, *6*, 6541–6545.

[5] Kairdolf, B. A.; Smith, A. M.; Stokes, T. H.; Wang, M. D.; Young, A. N.; Nie, S. M. Semiconductor quantum dots for bioimaging and biodiagnostic applications. *Annu. Rev. Anal. Chem.* **2013**, *6*, 143–162.

[6] Zhang, A. Q.; Lieber, C. M. Nano-bioelectronics. *Chem. Rev.* **2016**, *116*, 215–257.

[7] Feiner, R.; Dvir, T. Tissue-electronics interfaces: From implantable devices to engineered tissues. *Nat. Rev. Mater.* **2017**, *3*, 17076.

[8] Hendricks, M. P.; Sato, K.; Palmer, L. C.; Stupp, S. I. Supramolecular assembly of peptide amphiphiles. *Acc. Chem. Res.* **2017**, *50*, 2440–2448.

[9] Zhang, A. Q.; Zheng, G. F.; Lieber, C. M. *Nanowires*; Springer: Switzerland, 2016.

[10] Xia, Y. N.; Yang, P. D.; Sun, Y. G.; Wu, Y. Y.; Mayers, B.; Gates, B.; Yin, Y. D.; Kim, F.; Yan, H. Q. One-dimensional nanostructures: Synthesis, characterization, and applications. *Adv. Mater.* **2003**, *34*, 353–389.

[11] Levin, M.; Pezzulo, G.; Finkelstein, J. M. Endogenous bioelectric signaling networks: Exploiting voltage gradients for control of growth and form. *Annu. Rev. Biomed. Eng.* **2017**, *19*, 353–387.

[12] Kotov, N. A.; Winter, J. O.; Clements, I. P.; Jan, E.; Timko, B. P.; Campidelli, S.; Pathak, S.; Mazzatenta, A.; Lieber, C. M.; Prato, M. et al. Nanomaterials for neural interfaces. *Adv. Mater.* **2009**, *21*, 3970–4004.

[13] Nel, A. E.; Mädler, L.; Velegol, D.; Xia, T.; Hoek, E. M. V.; Somasundaran, P.; Klaessig, F.; Castranova, V.; Thompson, M. Understanding biophysicochemical interactions at the nano-bio interface. *Nat. Mater.* **2009**, *8*, 543–557.

[14] Mager, M. D.; LaPointe, V.; Stevens, M. M. Exploring and exploiting chemistry at the cell surface. *Nat. Chem.* **2011**, *3*, 582–589.

[15] Onclin, S.; Ravoo, B. J.; Reinhoudt, D. N. Engineering silicon oxide surfaces using self-assembled monolayers. *Angew. Chem., Int. Ed.* **2005**, *44*, 6282–6304.

[16] Love, J. C.; Estroff, L. A.; Kriebel, J. K.; Nuzzo, R. G.; Whitesides, G. M. Self-assembled monolayers of thiolates on metals as a form of nanotechnology. *Chem. Rev.* **2005**, *105*, 1103–1170.

[17] Cardenas-Benitez, B.; Djordjevic, I.; Hosseini, S.; Madou, M. J.; Martinez-Chapa, S. O. Review—Covalent functionalization of carbon nanomaterials for biosensor applications: An update. *J. Electrochem. Soc.* **2018**, *165*, B103–B117.

[18] Cohen-Karni, T.; Jeong, K. J.; Tsui, J. H.; Reznor, G.; Mustata, M.; Wanunu, M.; Graham, A.; Marks, C.; Bell, D. C.; Langer, R. et al. Nanocomposite gold-silk nanofibers. *Nano Lett.* **2012**, *12*, 5403–5406.

[19] Drelich, J.; Chibowski, E. Superhydrophilic and superwetting surfaces: Definition and mechanisms of control. *Langmuir* **2010**, *26*, 18621–18623.

[20] Zhang, M. Q.; Desai, T.; Ferrari, M. Proteins and cells on PEG immobilized silicon surfaces. *Biomaterials* **1998**, *19*, 953–960.

[21] Pan, H.; Xia, Y. F.; Qin, M.; Cao, Y.; Wang, W. A simple procedure to improve the surface passivation for single molecule fluorescence studies. *Phys. Biol.* **2015**, *12*, 045006.

[22] Marcon, L.; Addad, A.; Coffinier, Y.; Boukherroub, R. Cell micropatterning on superhydrophobic diamond nanowires. *Acta Biomater.* **2013**, *9*, 4585–4591.

[23] Valamehr, B.; Jonas, S. J.; Polleux, J.; Qiao, R.; Guo, S. L.; Gschweng, E. H.; Stiles, B.; Kam, K.; Luo, T. J. M.; Witte, O. N. et al. Hydrophobic surfaces for enhanced differentiation of embryonic stem cell-derived embryoid bodies. *Proc. Natl. Acad. Sci. USA* **2008**, *105*, 14459–14464.

[24] Nishino, T.; Meguro, M.; Nakamae, K.; Matsushita, M.; Ueda, Y. The lowest surface free energy based on $-CF_3$ alignment. *Langmuir* **1999**, *15*, 4321–4323.

[25] Coffinier, Y.; Janel, S.; Addad, A.; Blossey, R.; Gengembre, L.; Payen, E.; Boukherroub, R. Preparation of superhydrophobic silicon oxide nanowire surfaces. *Langmuir* **2007**, *23*, 1608–1611.

[26] Sun, T. L.; Feng, L.; Gao, X. F.; Jiang, L. Bioinspired surfaces with special wettability. *Acc. Chem. Res.* **2005**, *38*, 644–652.

[27] Falde, E. J.; Yohe, S. T.; Colson, Y. L.; Grinstaff, M. W. Superhydrophobic materials for biomedical applications. *Biomaterials* **2016**, *104*, 87–103.

[28] Wang, S. T.; Liu, K. S.; Yao, X.; Jiang, L. Bioinspired surfaces with superwettability: New insight on theory, design, and applications. *Chem. Rev.* **2015**, *115*, 8230–8293.

[29] Piret, G.; Galopin, E.; Coffinier, Y.; Boukherroub, R.; Legrand, D.; Slomianny, C. Culture of mammalian cells on patterned superhydrophilic/superhydrophobic silicon nanowire arrays. *Soft Matter* **2011**, *7*, 8642–8649.

[30] Lamour, G.; Eftekhari-Bafrooei, A.; Borguet, E.; Souès, S.; Hamraoui, A. Neuronal adhesion and differentiation driven by nanoscale surface free-energy gradients. *Biomaterials* **2010**, *31*, 3762–3771.

[31] Xu, L. P.; Meng, J. X.; Zhang, S. T.; Ma, X. L.; Wang, S. T. Amplified effect of surface charge on cell adhesion by nanostructures. *Nanoscale* **2016**, *8*, 12540–12543.

[32] Ning, R. Z.; Wang, S. Q.; Wu, J.; Wang, F.; Lin, J. M. ZnO nanowire arrays exhibit cytotoxic distinction to cancer cells with different surface charge density: Cytotoxicity is charge-dependent. *Small* **2014**, *10*, 4113–4117.

[33] Dante, S.; Petrelli, A.; Petrini, E. M.; Marotta, R.; Maccione, A.; Alabastri, A.; Quarta, A.; De Donato, F.; Ravasenga, T.; Sathya, A. et al. Selective targeting of neurons with inorganic nanoparticles: Revealing the crucial role of nanoparticle surface charge. *ACS Nano* **2017**, *11*, 6630–6640.

[34] Fabbro, A.; Bosi, S.; Ballerini, L.; Prato, M. Carbon nanotubes: Artificial nanomaterials to engineer single neurons and neuronal networks. *ACS Chem. Neurosci.* **2012**, *3*, 611–618.

[35] Zhou, X. J.; Moran-Mirabal, J. M.; Craighead, H. G.; McEuen, P. L. Supported lipid bilayer/carbon nanotube hybrids. *Nat. Nanotechnol.* **2007**, *2*, 185–190.

[36] Cellot, G.; Cilia, E.; Cipollone, S.; Rancic, V.; Sucapane, A.; Giordani, S.; Gambazzi, L.; Markram, H.; Grandolfo, M.; Scaini, D. et al. Carbon nanotubes might improve neuronal performance by favouring electrical shortcuts. *Nat. Nanotechnol.* **2009**, *4*, 126–133.

[37] Mazzatenta, A.; Giugliano, M.; Campidelli, S.; Gambazzi, L.; Businaro, L.; Markram, H.; Prato, M.; Ballerini, L. Interfacing neurons with carbon nanotubes: Electrical signal transfer and synaptic stimulation in cultured brain circuits. *J. Neurosci.* **2007**, *27*, 6931–6936.

[38] Santoro, F.; Zhao, W. T.; Joubert, L. M.; Duan, L. T.; Schnitker, J.; Van De Burgt, Y.; Lou, H. Y.; Liu, B. F.; Salleo, A.; Cui, L. F. et al. Revealing the cell-material interface with nanometer resolution by focused ion beam/scanning electron microscopy. *ACS Nano* **2017**, *11*, 8320–8328.

[39] Hanson, L.; Lin, Z. C.; Xie, C.; Cui, Y.; Cui, B. X. Characterization of the cell-nanopillar interface by transmission electron microscopy. *Nano Lett.* **2012**, *12*, 5815–5820.

[40] Lovat, V.; Pantarotto, D.; Lagostena, L.; Cacciari, B.; Grandolfo, M.; Righi, M.; Spalluto, G.; Prato, M.; Ballerini, L. Carbon nanotube substrates boost neuronal electrical signaling. *Nano Lett.* **2005**, *5*, 1107–1110.

[41] Cellot, G.; Toma, F. M.; Kasap Varley, Z.; Laishram, J.; Villari, A.; Quintana, M.; Cipollone, S.; Prato, M.; Ballerini, L. Carbon nanotube scaffolds tune synaptic strength in cultured neural circuits: Novel frontiers in nanomaterial-tissue interactions. *J. Neurosci.* **2011**, *31*, 12945–12953.

[42] Fabbro, A.; Sucapane, A.; Toma, F. M.; Calura, E.; Rizzetto, L.; Carrieri, C.; Roncaglia, P.; Martinelli, V.; Scaini, D.; Masten, L. et al. Adhesion to carbon nanotube conductive scaffolds forces action-potential appearance in immature rat spinal neurons. *PLoS One* **2013**, *8*, e73621.

[43] Bettinger, C. J.; Langer, R.; Borenstein, J. T. Engineering substrate topography at the micro- and nanoscale to control cell function. *Angew. Chem., Int. Ed.* **2009**, *48*, 5406–5415.

[44] Case, L. B.; Baird, M. A.; Shtengel, G.; Campbell, S. L.; Hess, H. F.; Davidson, M. W.; Waterman, C. M. Molecular mechanism of vinculin activation and nanoscale spatial organization in focal adhesions. *Nat. Cell Biol.* **2015**, *17*, 880–892.

[45] Park, J.; Bauer, S.; Von Der Mark, K.; Schmuki, P. Nanosize and vitality: TiO_2 nanotube diameter directs cell fate. *Nano Lett.* **2007**, *7*, 1686–1691.

[46] Park, Y. S.; Yoon, S. Y.; Park, J. S.; Lee, J. S. Deflection induced cellular focal adhesion and anisotropic growth on vertically aligned silicon nanowires with differing elasticity. *NPG Asia Mater.* **2016**, *8*, e249.

[47] Erickson, J.; Tooker, A.; Tai, Y. C.; Pine, J. Caged neuron mea: A system for long-term investigation of cultured neural network connectivity. *J. Neurosci. Methods.* **2008**, *175*, 1–16.

[48] Xie, C.; Hanson, L.; Xie, W. J.; Lin, Z. L.; Cui, B. X.; Cui, Y. Noninvasive neuron pinning with nanopillar arrays. *Nano Lett.* **2010**, *10*, 4020–4024.

[49] Qi, S. J.; Yi, C. Q.; Ji, S. L.; Fong, C. C.; Yang, M. S. Cell adhesion and spreading behavior on vertically aligned silicon nanowire arrays. *ACS Appl. Mater. Interfaces* **2009**, *1*, 30–34.

[50] Persson, H.; Li, Z.; Tegenfeldt, J. O.; Oredsson, S.; Prinz, C. N. From immobilized cells to motile cells on a bed-of-nails: Effects of vertical nanowire array density on cell behaviour. *Sci. Rep.* **2015**, *5*, 18535.

[51] Li, Z.; Song, J. H.; Mantini, G.; Lu, M. Y.; Fang, H.; Falconi, C.; Chen, L. J.; Wang, Z. L. Quantifying the traction force of a single cell by aligned silicon nanowire array. *Nano Lett.* **2009**, *9*, 3575–3580.

[52] Teixeira, A. I.; Abrams, G. A.; Bertics, P. J.; Murphy, C. J.; Nealey, P. F. Epithelial contact guidance on well-defined micro- and nanostructured substrates. *J. Cell Sci.* **2003**, *116*, 1881–1892.

[53] Gautam, V.; Naureen, S.; Shahid, N.; Gao, Q.; Wang, Y.; Nisbet, D.; Jagadish, C.; Daria, V. R. Engineering highly interconnected neuronal networks on nanowire scaffolds. *Nano Lett.* **2017**, *17*, 3369–3375.

[54] Brammer, K. S.; Choi, C.; Frandsen, C. J.; Oh, S.; Jin, S. Hydrophobic nanopillars initiate mesenchymal stem cell aggregation and osteo-differentiation. *Acta Biomater.* **2011**, *7*, 683–690.

[55] Bauer, S.; Park, J.; Von Der Mark, K.; Schmuki, P. Improved attachment of mesenchymal stem cells on super-hydrophobic TiO_2 nanotubes. *Acta Biomater.* **2008**, *4*, 1576–1582.

[56] Zhang, Z.; Fu, Y.; Yu, W.; Qin, X. Y.; Xue, Z. J.; Liu, Y.; Luo, D.; Yan, C.; Sun, X. H.; Wang, T. Dynamically regulated Ag nanowire arrays for detecting molecular information of substrate-induced stretched cell growth. *Adv. Mater.* **2016**, *28*, 9589–9595.

[57] Bucaro, M. A.; Vasquez, Y.; Hatton, B. D.; Aizenberg, J. Fine-tuning the degree of stem cell polarization and alignment on ordered arrays of high-aspect-ratio nanopillars. *ACS Nano* **2012**, *6*, 6222–6230.

[58] Piret, G.; Perez, M. T.; Prinz, C. N. Support of neuronal growth over glial growth and guidance of optic nerve axons by vertical nanowire arrays. *ACS Appl. Mater. Interfaces* **2015**, *7*, 18944–18948.

[59] Yan, Q. T.; Fang, L. P.; Wei, J. Y.; Xiao, G. P.; Lv, M. H.; Ma, Q. H.; Liu, C. F.; Wang, W. Silicon nanowires enhanced proliferation and neuronal differentiation of neural stem cell with vertically surface microenvironment. *J. Biomater. Sci. Polym. Ed.* **2017**, *28*, 1394–1407.

[60] Marei, H. E.; Elnegiry, A. A.; Zaghloul, A.; Althani, A.; Afifi, N.; Abd-Elmaksoud, A.; Farag, A.; Lashen, S.; Rezk, S.; Shouman, Z. et al. Nanotubes impregnated human olfactory bulb neural stem cells promote neuronal differentiation in trimethyltin-induced neurodegeneration rat model. *J. Cell.*

Physiol. **2017**, *232*, 3586–3597.

[61] Nayak, T. R.; Jian, L.; Phua, L. C.; Ho, H. K.; Ren, Y. P.; Pastorin, G. Thin films of functionalized multiwalled carbon nanotubes as suitable scaffold materials for stem cells proliferation and bone formation. *ACS Nano* **2010**, *4*, 7717–7725.

[62] Oh, S.; Brammer, K. S.; Li, Y. S. J.; Teng, D. Y.; Engler, A. J.; Chien, S.; Jin, S. Stem cell fate dictated solely by altered nanotube dimension. *Proc*. *Natl*. *Acad*. *Sci*. *USA* **2009**, *106*, 2130–2135.

[63] Abbott, J.; Ye, T. Y.; Ham, D.; Park, H. Optimizing nano-electrode arrays for scalable intracellular electrophysiology. *Acc*. *Chem*. *Res*. **2018**, *51*, 600–608.

[64] Qing, Q.; Jiang, Z.; Xu, L.; Gao, R. X.; Mai, L. Q.; Lieber, C. M. Free-standing kinked nanowire transistor probes for targeted intracellular recording in three dimensions. *Nat*. *Nanotechnol*. **2014**, *9*, 142–147.

[65] Hai, A.; Shappir, J.; Spira, M. E. In-cell recordings by extracellular microelectrodes. *Nat*. *Methods* **2010**, *7*, 200–202.

[66] Dipalo, M.; Amin, H.; Lovato, L.; Moia, F.; Caprettini, V.; Messina, G. C.; Tantussi, F.; Berdondini, L.; De Angelis, F. Intracellular and extracellular recording of spontaneous action potentials in mammalian neurons and cardiac cells with 3D plasmonic nanoelectrodes. *Nano Lett*, **2017**, *17*, 3932–3939.

[67] Xie, C.; Lin, Z. L.; Hanson, L.; Cui, Y.; Cui, B. X. Intracellular recording of action potentials by nanopillar electroporation. *Nat*. *Nanotechnol*. **2012**, *7*, 185–190.

[68] Lin, Z. C.; Xie, C.; Osakada, Y.; Cui, Y.; Cui, B. X. Iridium oxide nanotube electrodes for sensitive and prolonged intracellular measurement of action potentials. *Nat*. *Commun*. **2014**, *5*, 3206.

[69] Hällström, W.; Mårtensson, T.; Prinz, C.; Gustavsson, P.; Montelius, L.; Samuelson, L.; Kanje, M. Gallium phosphide nanowires as a substrate for cultured neurons. *Nano Lett*. **2007**, *7*, 2960–2965.

[70] Kim, W.; Ng, J. K.; Kunitake, M. E.; Conklin, B. R.; Yang, P. D. Interfacing silicon nanowires with mammalian cells. *J*. *Am*. *Chem*. *Soc*. **2007**, *129*, 7228–7229.

[71] Xie, X.; Xu, A. M.; Angle, M. R.; Tayebi, N.; Verma, P.; Melosh, N. A. Mechanical model of vertical nanowire cell penetration. *Nano Lett*. **2013**, *13*, 6002–6008.

[72] Huang, C. J.; Zhang, Y.; Yuan, H. Y.; Gao, H. J.; Zhang, S. L. Role of nanoparticle geometry in endocytosis: Laying down to stand up. *Nano Lett*. **2013**, *13*, 4546–4550.

[73] Yaron, P. N.; Holt, B. D.; Short, P. A.; Lösche, M.; Islam, M. F.; Dahl, K. N. Single wall carbon nanotubes enter cells by endocytosis and not membrane penetration. *J*. *Nano-biotechnology*. **2011**, *9*, 45.

[74] Zimmerman, J. F.; Parameswaran, R.; Murray, G.; Wang, Y. C.; Burke, M.; Tian, B. Z. Cellular uptake and dynamics of unlabeled freestanding silicon nanowires. *Sci*. *Adv*. **2016**, *2*, e1601039.

[75] Lee, J. H.; Zhang, A. Q.; You, S. S.; Lieber, C. M. Spontaneous internalization of cell penetrating peptide-modified nanowires into primary neurons. *Nano Lett*. **2016**, *16*, 1509–1513.

[76] Khlebtsov, N.; Dykman, L. Biodistribution and toxicity of engineered gold nanoparticles: A review of *in vitro* and *in vivo* studies. *Chem*. *Soc*. *Rev*. **2011**, *40*, 1647–1671.

[77] Petros, R. A.; DeSimone, J. M. Strategies in the design of nanoparticles for therapeutic applications. *Nat*. *Rev*. *Drug Discov*. **2010**, *9*, 615–627.

[78] Shi, X. H.; Von Dem Bussche, A.; Hurt, R. H.; Kane, A. B.; Gao, H. J. Cell entry of one-dimensional nanomaterials occurs by tip recognition and rotation. *Nat*. *Nanotechnol*. **2011**, *6*, 714–719.

[79] Hamilton Jr, R. F.; Wu, N. Q.; Porter, D.; Buford, M.; Wolfarth, M.; Holian, A. Particle length-dependent titanium dioxide nanomaterials toxicity and bioactivity. *Part*. *Fibre Toxicol*. **2009**, *6*, 35.

[80] Ji, Z. X.; Wang, X.; Zhang, H. Y.; Lin, S. J.; Meng, H.; Sun, B. B.; George, S.; Xia, T.; Nel, A. E.; Zink, J. I. Designed synthesis of CeO_2 nanorods and nanowires for studying toxicological effects of high aspect ratio nanomaterials. *ACS Nano* **2012**, *6*, 5366–5380.

[81] Felix, L. P.; Perez, J. E.; Contreras, M. F.; Ravasi, T.; Kosel, J. Cytotoxic effects of nickel nanowires in human fibroblasts. *Toxicol*. *Rep*. **2016**, *3*, 373–380.

[82] Poland, C. A.; Duffin, R.; Kinloch, I.; Maynard, A.; Wallace, W. A. H.; Seaton, A.; Stone, V.; Brown, S.; MacNee, W.; Donaldson, K. Carbon nanotubes introduced into the abdominal cavity of mice show asbestos-like pathogenicity in a pilot study. *Nat*. *Nanotechnol*. **2008**, *3*, 423–428.

[83] Roberts, J. R.; Mercer, R. R.; Chapman, R. S.; Cohen, G. M.; Bangsaruntip, S.; Schwegler-Berry, D.; Scabilloni, J. F.; Castranova, V.; Antonini, J. M.; Leonard, S. S. Pulmonary toxicity, distribution, and clearance of intratracheally instilled silicon nanowires in rats. *J*. *Nanomater*. **2012**, *2012*, 398302.

[84] Silva, R. M.; Xu, J. Y.; Saiki, C.; Anderson, D. S.; Franzi, L. M.; Vulpe, C. D.; Gilbert, B.; Van Winkle, L. S.; Pinkerton, K. E. Short versus long silver nanowires: A comparison of *in vivo* pulmonary effects post instillation. *Part*. *Fibre Toxicol*. **2014**, *11*, 52.

[85] Verma, N. K.; Conroy, J.; Lyons, P. E.; Coleman, J.; O'Sullivan, M. P.; Kornfeld, H.; Kelleher, D.; Volkov, Y. Autophagy induction by silver nanowires: A new aspect in the biocompatibility assessment of nanocomposite thin films. *Toxicol*. *Appl*. *Pharmacol*. **2012**, *264*, 451–461.

[86] Dvir, T.; Timko, B. P.; Brigham, M. D.; Naik, S. R.; Karajanagi, S. S.; Levy, O.; Jin, H. W.; Parker, K. K.; Langer, R.; Kohane, D. S. Nanowired three-dimensional cardiac patches. *Nat*. *Nanotechnol*. **2011**, *6*, 720–725.

[87] Dai, X. C.; Zhou, W.; Gao, T.; Liu, J.; Lieber, C. M. Three-dimensional mapping and regulation of action potential propagation in nanoelectronics-innervated tissues. *Nat*. *Nanotechnol*. **2016**, *11*, 776–782.

[88] Kohane, D. S.; Langer, R. Biocompatibility and drug delivery systems. *Chem*. *Sci*. **2010**, *1*, 441–446.

[89] Mahmoudi, M.; Yu, M.; Serpooshan, V.; Wu, J. C.; Langer, R.; Lee, R. T.; Karp, J. M.; Farokhzad, O. C. Multiscale technologies for treatment of ischemic cardiomyopathy. *Nat*. *Nanotechnol*. **2017**, *12*, 845–855.

[90] Ruvinov, E.; Cohen, S. Alginate biomaterial for the treatment of myocardial infarction: Progress, translational strategies, and clinical outlook: From ocean algae to patient bedside. *Adv*. *Drug Deliv*. *Rev*. **2016**, *96*, 54–76.

[91] You, J. O.; Rafat, M.; Ye, G. J. C.; Auguste, D. T. Nanoengineering the heart: Conductive scaffolds enhance connexin 43 expression. *Nano Lett*. **2011**, *11*, 3643–3648.

[92] Navaei, A.; Saini, H.; Christenson, W.; Sullivan, R. T.; Ros, R.; Nikkhah, M. Gold nanorod-incorporated gelatin-based conductive hydrogels for engineering cardiac tissue constructs. *Acta Biomater*. **2016**, *41*, 133–146.

[93] Zhu, K.; Shin, S. R.; Van Kempen, T.; Li, Y. C.; Ponraj, V.; Nasajpour, A.; Mandla, S.; Hu, N.; Liu, X.; Leijten, J. et al. Gold nanocomposite bioink for printing 3D cardiac constructs. *Adv*. *Funct*. *Mater*. **2017**, 1605352.

[94] Shin, S. R.; Jung, S. M.; Zalabany, M.; Kim, K.; Zorlutuna, P.; Kim, S. B.; Nikkhah, M.; Khabiry, M.; Azize, M.; Kong, J. et al. Carbon-nanotube-embedded hydrogel sheets for engineering cardiac constructs and bioactuators. *ACS Nano* **2013**, *7*, 2369–2380.

[95] Tan, Y.; Richards, D.; Xu, R. Y.; Stewart-Clark, S.; Mani, S. K.; Borg, T. K.; Menick, D. R.; Tian, B. Z.; Mei, Y. Silicon nanowire-induced maturation of cardiomyocytes derived from human induced pluripotent stem cells. *Nano Lett*. **2015**, *15*, 2765–2772.

[96] Richards, D. J.; Tan, Y.; Coyle, R.; Li, Y.; Xu, R. Y.; Yeung, N.; Parker, A.; Menick, D. R.; Tian, B. Z.; Mei, Y. Nanowires and electrical stimulation synergistically improve functions of hiPSC cardiac spheroids. *Nano Lett*. **2016**, *16*, 4670–4678.

[97] Wu, Y.; Guo, L. Enhancement of intercellular electrical synchronization by conductive materials in cardiac tissue engineering. *IEEE Trans*. *Biomed*. *Eng*. **2018**, *65*, 264–272.

[98] Zhu, W.; Ye, T.; Lee, S. J.; Cui, H. T.; Miao, S. D.; Zhou, X.; Shuai, D. M.; Zhang, L. G. Enhanced neural stem cell functions in conductive annealed carbon nanofibrous scaffolds with electrical stimulation. *Nanomedicine*: *Nanotechnol*., *Biol*. *Med*., in press, DOI: 10.1016/j.nano.2017.03.018.

[99] Koppes, A. N.; Keating, K. W.; McGregor, A. L.; Koppes, R. A.; Kearns, K. R.; Ziemba, A. M.; McKay, C. A.; Zuidema, J. M.; Rivet, C. J.; Gilbert, R. J. et al. Robust neurite extension following exogenous electrical stimulation within single walled carbon nanotube-composite hydrogels. *Acta Biomater*. **2016**, *39*, 34–43.

[100] Fabbro, A.; Villari, A.; Laishram, J.; Scaini, D.; Toma, F. M.; Turco, A.; Prato, M.; Ballerini, L. Spinal cord explants use carbon nanotube interfaces to enhance neurite outgrowth and to fortify synaptic inputs. *ACS Nano* **2012**, *6*, 2041–2055.

[101] Qian, Y.; Zhao, X. T.; Han, Q. X.; Chen, W.; Li, H.; Yuan, W. E. An integrated multi-layer 3D-fabrication of PDA/RGD coated graphene loaded PCL nanoscaffold for peripheral nerve restoration. *Nat*. *Commun*. **2018**, *9*, 323.

[102] Bian, W. N.; Jackman, C. P.; Bursac, N. Controlling the structural and functional anisotropy of engineered cardiac tissues. *Biofabrication* **2014**, *6*, 024109.

[103] Jana, S.; Levengood, S. K. L.; Zhang, M. Q. Anisotropic materials for skeletal-muscle-tissue engineering. *Adv*. *Mater*. **2016**, *28*, 10588–10612.

[104] De France, K. J.; Yager, K. G.; Chan, K. J. W.; Corbett, B.; Cranston, E. D.; Hoare, T. Injectable anisotropic nanocomposite hydrogels direct *in situ* growth and alignment of myotubes. *Nano Lett*. **2017**, *17*, 6487–6495.

[105] Ozasa, R.; Matsugaki, A.; Isobe, Y.; Saku, T.; Yun, H. S.; Nakano, T. Construction of human induced pluripotent stem cell-derived oriented bone matrix microstructure by using *in vitro* engineered anisotropic culture model. *J*. *Biomed*. *Mater*. *Res*. *A*. **2018**, *106*, 360–369.

[106] Rose, J. C.; Cámara-Torres, M.; Rahimi, K.; Köhler, J.; Möller, M.; De Laporte, L. Nerve cells decide to orient inside an injectable hydrogel with minimal structural guidance. *Nano Lett*. **2017**, *17*, 3782–3791.

[107] Wu, Y. B.; Wang, L.; Guo, B. L.; Ma, P. X. Interwoven aligned conductive nanofiber yarn/hydrogel composite scaffolds for engineered 3D cardiac anisotropy. *ACS Nano* **2017**, *11*, 5646–5659.

[108] Kimura, T.; Ago, H.; Tobita, M.; Ohshima, S.; Kyotani, M.; Yumura, M. Polymer composites of carbon nanotubes aligned by a magnetic field. *Adv*. *Mater*. **2002**, *14*, 1380–1383.

[109] Burrows, N. D.; Vartanian, A. M.; Abadeer, N. S.; Grzincic, E. M.; Jacob, L. M.; Lin, W.; Li, J.; Dennison, J. M.; Hinman, J. G.; Murphy, C. J. Anisotropic nanoparticles and anisotropic surface chemistry. *J*. *Phys*. *Chem*. *Lett*. **2016**, *7*, 632–641.

[110] Egert, U.; Heck, D.; Aertsen, A. Two-dimensional monitoring of spiking networks in acute brain slices. *Exp. Brain Res.* **2002**, *142*, 268–274.

[111] Stangl, C.; Fromherz, P. Neuronal field potential in acute hippocampus slice recorded with transistor and micropipette electrode. *Eur. J. Neurosci.* **2008**, *27*, 958–964.

[112] Yu, G. H.; Lieber, C. M. Assembly and integration of semiconductor nanowires for functional nanosystems. *Pure Appl. Chem.* **2010**, *82*, 2295–2314.

[113] Timko, B. P.; Cohen-Karni, T.; Qing, Q.; Tian, B. Z.; Lieber, C. M. Design and implementation of functional nanoelectronic interfaces with biomolecules, cells, and tissue using nanowire device arrays. *IEEE Trans. Nanotechnol.* **2010**, *9*, 269–280.

[114] Timko, B. P.; Cohen-Karni, T.; Yu, G. H.; Qing, Q.; Tian, B. Z.; Lieber, C. M. Electrical recording from hearts with flexible nanowire device arrays. *Nano Lett.* **2009**, *9*, 914–918.

[115] Cohen-Karni, T.; Timko, B. P.; Weiss, L. E.; Lieber, C. M. Flexible electrical recording from cells using nanowire transistor arrays. *Proc. Natl. Acad. Sci. USA* **2009**, *106*, 7309–7313.

[116] Tian, B. Z.; Cohen-Karni, T.; Qing, Q.; Duan, X. J.; Xie, P.; Lieber, C. M. Three-dimensional, flexible nanoscale field-effect transistors as localized bioprobes. *Science* **2010**, *329*, 830–834.

[117] Patolsky, F.; Timko, B. P.; Yu, G. H.; Fang, Y.; Greytak, A. B.; Zheng, G. F.; Lieber, C. M. Detection, stimulation, and inhibition of neuronal signals with high-density nanowire transistor arrays. *Science* **2006**, *313*, 1100–1104.

[118] Eschermann, J. F.; Stockmann, R.; Hueske, M.; Vu, X. T.; Ingebrandt, S.; Offenhäusser, A. Action potentials of HL-1 cells recorded with silicon nanowire transistors. *Appl. Phys. Lett.* **2009**, *95*, 083703.

[119] Pui, T. S.; Agarwal, A.; Ye, F.; Balasubramanian, N.; Chen, P. CMOS-compatible nanowire sensor arrays for detection of cellular bioelectricity. *Small* **2009**, *5*, 208–212.

[120] Massobrio, P.; Massobrio, G.; Martinoia, S. Interfacing cultured neurons to microtransducers arrays: A review of the neuro-electronic junction models. *Front. Neurosci.* **2016**, *10*, 282.

[121] Offenhäusser, A.; Knoll, W. Cell-transistor hybrid systems and their potential applications. *Trends Biotechnol.* **2001**, *19*, 62–66.

[122] Ingebrandt, S.; Yeung, C. K.; Krause, M.; Offenhäusser, A. Cardiomyocyte-transistor-hybrids for sensor application. *Biosens. Bioelectron.* **2001**, *16*, 565–570.

[123] Braun, D.; Fromherz, P. Imaging neuronal seal resistance on silicon chip using fluorescent voltage-sensitive dye. *Biophys. J.* **2004**, *87*, 1351–1359.

[124] Cohen-Karni, T.; Casanova, D.; Cahoon, J. F.; Qing, Q.; Bell, D. C.; Lieber, C. M. Synthetically encoded ultrashort-channel nanowire transistors for fast, pointlike cellular signal detection. *Nano Lett.* **2012**, *12*, 2639–2644.

[125] Xu, L.; Jiang, Z.; Mai, L. Q.; Qing, Q. Multiplexed free-standing nanowire transistor bioprobe for intracellular recording: A general fabrication strategy. *Nano Lett.* **2014**, *14*, 3602–3607.

[126] Duan, X. J.; Gao, R. X.; Xie, P.; Cohen-Karni, T.; Qing, Q.; Choe, H. S.; Tian, B. Z.; Jiang, X. C.; Lieber, C. M. Intracellular recordings of action potentials by an extracellular nanoscale field-effect transistor. *Nat. Nanotechnol.* **2012**, *7*, 174–179.

[127] Gao, R. X.; Strehle, S.; Tian, B. Z.; Cohen-Karni, T.; Xie, P.; Duan, X. J.; Qing, Q.; Lieber, C. M. Outside looking in: Nanotube transistor intracellular sensors. *Nano Lett.* **2012**, *12*, 3329–3333.

[128] Qing, Q.; Pal, S. K.; Tian, B. Z.; Duan, X. J.; Timko, B. P.; Cohen-Karni, T.; Murthy, V. N.; Lieber, C. M. Nanowire transistor arrays for mapping neural circuits in acute brain slices. *Proc. Natl. Acad. Sci. USA* **2010**, *107*, 1882–1887.

[129] Tian, B. Z.; Liu, J.; Dvir, T.; Jin, L. H.; Tsui, J. H.; Qing, Q.; Suo, Z. G.; Langer, R.; Kohane, D. S.; Lieber, C. M. Macroporous nanowire nanoelectronic scaffolds for synthetic tissues. *Nat. Mater.* **2012**, *11*, 986–994.

[130] Liu, J.; Fu, T. M.; Cheng, Z. G.; Hong, G. S.; Zhou, T.; Jin, L. H.; Duvvuri, M.; Jiang, Z.; Kruskal, P.; Xie, C. et al. Syringe-injectable electronics. *Nat. Nanotechnol.* **2015**, *10*, 629–636.

[131] Hong, G. S.; Fu, T. M.; Zhou, T.; Schuhmann, T. G.; Huang, J. L.; Lieber, C. M. Syringe injectable electronics: Precise targeted delivery with quantitative input/output connectivity. *Nano Lett.* **2015**, *15*, 6979–6984.

[132] Schuhmann, T. G.; Yao, J.; Hong, G. S.; Fu, T. M.; Lieber, C. M. Syringe-injectable electronics with a plug-and-play input/output interface. *Nano Lett.* **2017**, *17*, 5836–5842.

[133] Zhou, T.; Hong, G. S.; Fu, T. M.; Yang, X.; Schuhmann, T. G.; Viveros, R. D.; Lieber, C. M. Syringe-injectable mesh electronics integrate seamlessly with minimal chronic immune response in the brain. *Proc. Natl. Acad. Sci. USA* **2017**, *114*, 5894–5899.

[134] Fu, T. M.; Hong, G. S.; Zhou, T.; Schuhmann, T. G.; Viveros, R. D.; Lieber, C. M. Stable long-term chronic brain mapping at the single-neuron level. *Nat. Methods* **2016**, *13*, 875–882.

[135] Fu, T. M.; Hong, G. S.; Viveros, R. D.; Zhou, T.; Lieber, C. M. Highly scalable multichannel mesh electronics for stable chronic brain electrophysiology. *Proc. Natl. Acad.*

Sci. *USA* **2017**, *21*, E10046–E10055.

[136] Yin, L.; Farimani, A. B.; Min, K.; Vishal, N.; Lam, J.; Lee, Y. K.; Aluru, N. R.; Rogers, J. A. Mechanisms for hydrolysis of silicon nanomembranes as used in bioresorbable electronics. *Adv*. *Mater*. **2015**, *27*, 1857–1864.

[137] Lee, Y. K.; Yu, K. J.; Song, E. M.; Barati Farimani, A.; Vitale, F.; Xie, Z. Q.; Yoon, Y.; Kim, Y.; Richardson, A.; Luan, H. W. et al. Dissolution of monocrystalline silicon nanomembranes and their use as encapsulation layers and electrical interfaces in water-soluble electronics. *ACS Nano* **2017**, *11*, 12562–12572.

[138] Kang, S. K.; Murphy, R. K. J.; Hwang, S. W.; Lee, S. M.; Harburg, D. V.; Krueger, N. A.; Shin, J.; Gamble, P.; Cheng, H. Y.; Yu, S. et al. Bioresorbable silicon electronic sensors for the brain. *Nature* **2016**, *530*, 71–76.

[139] Zhou, W.; Dai, X. C.; Fu, T. M.; Xie, C.; Liu, J.; Lieber, C. M. Long term stability of nanowire nanoelectronics in physiological environments. *Nano Lett*. **2014**, *14*, 1614–1619.

[140] Lin, Z. C.; McGuire, A. F.; Burridge, P. W.; Matsa, E.; Lou, H. Y.; Wu, J. C.; Cui, B. X. Accurate nanoelectrode recording of human pluripotent stem cell-derived cardiomyocytes for assaying drugs and modeling disease. *Microsyst*. *Nanoeng* **2017**, *3*, 16080.

[141] Robinson, J. T.; Jorgolli, M.; Shalek, A. K.; Yoon, M. H.; Gertner, R. S.; Park, H. Vertical nanowire electrode arrays as a scalable platform for intracellular interfacing to neuronal circuits. *Nat*. *Nanotechnol*. **2012**, *7*, 180–184.

[142] Liu, R.; Chen, R. J.; Elthakeb, A. T.; Lee, S. H.; Hinckley, S.; Khraiche, M. L.; Scott, J.; Pre, D.; Hwang, Y.; Tanaka, A. et al. High density individually addressable nanowire arrays record intracellular activity from primary rodent and human stem cell derived neurons. *Nano Lett*. **2017**, *17*, 2757–2764.

[143] Kang, M.; Jung, S.; Zhang, H. N.; Kang, T.; Kang, H.; Yoo, Y.; Hong, J. P.; Ahn, J. P.; Kwak, J.; Jeon, D. et al. Subcellular neural probes from single-crystal gold nanowires. *ACS Nano* **2014**, *8*, 8182–8189.

[144] Lugo, K.; Miao, X. Y.; Rieke, F.; Lin, L. Y. Remote switching of cellular activity and cell signaling using light in conjunction with quantum dots. *Biomed*. *Opt*. *Express* **2012**, *3*, 447–454.

[145] Pappas, T. C.; Wickramanyake, W. M. S.; Jan, E.; Motamedi, M.; Brodwick, M.; Kotov, N. A. Nanoscale engineering of a cellular interface with semiconductor nanoparticle films for photoelectric stimulation of neurons. *Nano Lett*. **2007**, *7*, 513–519.

[146] Parameswaran, R.; Carvalho-de-Souza, J. L.; Jiang, Y. W.; Burke, M. J.; Zimmerman, J. F.; Koehler, K.; Phillips, A. W.; Yi, J.; Adams, E. J.; Bezanilla, F. et al. Photoelectrochemical modulation of neuronal activity with free-standing coaxial silicon nanowires. *Nat*. *Nanotechnol*. **2018**, *13*, 260–266.

[147] Wang, W. Y.; Sedykh, A.; Sun, H. N.; Zhao, L. L.; Russo, D. P.; Zhou, H. Y.; Yan, B.; Zhu, H. Predicting nano-bio interactions by integrating nanoparticle libraries and quantitative nanostructure activity relationship modeling. *ACS Nano* **2017**, *11*, 12641–12649.

[148] Vila, F. D.; Hayashi, S. T.; Moore, J. M.; Rehr, J. J. Molecular dynamics simulations of supported Pt nanoparticles with a hybrid sutton-chen potential. *J*. *Phys*. *Chem*. *C*. **2016**, *120*, 14883–14891.

[149] Khalkhali, M.; Kazemi, N.; Zhang, H.; Liu, Q. X. Wetting at the nanoscale: A molecular dynamics study. *J*. *Chem*. *Phys*. **2017**, *146*, 114704.

[150] Shen, Z. Q.; Ye, H. L.; Li, Y. Understanding receptor-mediated endocytosis of elastic nanoparticles through coarse grained molecular dynamic simulation. *Phys*. *Chem*. *Chem*. *Phys*. **2018**, *20*, 16372–16385.

[151] Cherkasov, A.; Muratov, E. N.; Fourches, D.; Varnek, A.; Baskin, I. I.; Cronin, M.; Dearden, J.; Gramatica, P.; Martin, Y. C.; Todeschini, R. et al. QSAR modeling: Where have you been? Where are you going to? *J*. *Med*. *Chem*. **2014**, *57*, 4977–5010.

[152] Puzyn, T.; Jeliazkova, N.; Sarimveis, H.; Marchese Robinson, R. L.; Lobaskin, V.; Rallo, R.; Richarz, A. N.; Gajewicz, A.; Papadopulos, M. G.; Hastings, J. et al. Perspectives from the nanosafety modelling cluster on the validation criteria for (Q)SAR models used in nanotechnology. *Food Chem*. *Toxicol*. **2018**, *112*, 478–494.

[153] Bai, X.; Liu, F.; Liu, Y.; Li, C.; Wang, S. Q.; Zhou, H. Y.; Wang, W. Y.; Zhu, H.; Winkler, D. A.; Yan, B. Toward a systematic exploration of nano-bio interactions. *Toxicol*. *Appl*. *Pharmacol*. **2017**, *323*, 66–73.

[154] Wu, L.; Zhang, Y.; Zhang, C. K.; Cui, X. H.; Zhai, S. M.; Liu, Y.; Li, C. L.; Zhu, H.; Qu, G. B.; Jiang, G. B. et al. Tuning cell autophagy by diversifying carbon nanotube surface chemistry. *ACS Nano* **2014**, *8*, 2087–2099.

[155] Zhang, Y.; Wang, Y. B.; Liu, A. J.; Xu, S. L.; Zhao, B.; Zhang, Y.; Zou, H. F.; Wang, W. Y.; Zhu, H.; Yan, B. Modulation of carbon nanotubes' perturbation to the metabolic activity of CYP3A4 in the liver. *Adv*. *Funct*. *Mater*. **2016**, *26*, 841–850.

[156] Sizochenko, N.; Leszczynska, D.; Leszczynski, J. Modeling of interactions between the zebrafish hatching enzyme ZHE1 and a series of metal oxide nanoparticles: Nano-QSAR and causal analysis of inactivation mechanisms. *Nanomaterials* **2017**, *7*, 330.

[157] Trinh, T. X.; Choi, J. S.; Jeon, H.; Byun, H. G.; Yoon, T. H.; Kim, J. Quasi-SMILES-based nano-quantitative structure-

activity relationship model to predict the cytotoxicity of multiwalled carbon nanotubes to human lung cells. *Chem. Res. Toxicol*. **2018**, *31*, 183–190.

[158] Pratihar, S.; Kim, N.; Kohale, S. C.; Hase, W. L. Mechanistic details of energy transfer and soft landing in ala_2-H^+ collisions with a F-SAM surface. *Phys. Chem. Chem. Phys*. **2015**, *17*, 24576–24586.

[159] Pratihar, S.; Kohale, S. C.; Bhakta, D. G.; Laskin, J.; Hase, W. L. Dynamics o f energy transfer and soft-landing in collisions of protonated dialanine with perfluorinated self-assembled monolayer surfaces. *Phys. Chem. Chem. Phys*. **2014**, *16*, 23769–23778.

[160] Bajaj, P.; Schweller, R. M.; Khademhosseini, A.; West, J. L.; Bashir, R. 3D biofabrication strategies for tissue engineering and regenerative medicine. *Annu. Rev. Biomed. Eng*. **2014**, *16*, 247–276.

[161] Fan, F. R.; Tang, W.; Wang, Z. L. Flexible nanogenerators for energy harvesting and self-powered electronics. *Adv. Mater*. **2016**, *28*, 4283–4305.

[162] Yan, R. X.; Gargas, D.; Yang, P. D. Nanowire photonics. *Nat. Photonics* **2009**, *3*, 569–576.

[163] Kang, S. K.; Koo, J.; Lee, Y. K.; Rogers, J. A. Advanced materials and devices for bioresorbable electronics. *Acc. Chem. Res*. **2018**, *51*, 988–998.

[164] Wang, S. R.; Ghezzi, C. E.; Gomes, R.; Pollard, R. E.; Funderburgh, J. L.; Kaplan, D. L. *In vitro* 3D corneal tissue model with epithelium, stroma, and innervation. *Biomaterials* **2017**, *112*, 1–9.

[165] Tang-Schomer, M. D.; White, J. D.; Tien, L. W.; Schmitt, L. I.; Valentin, T. M.; Graziano, D. J.; Hopkins, A. M.; Omenetto, F. G.; Haydon, P. G.; Kaplan, D. L. Bioengineered functional brain-like cortical tissue. *Proc. Natl. Acad. Sci. USA* **2014**, *111*, 13811–13816.

[166] Chen, Y.; Lin, Y. N.; Davis, K. M.; Wang, Q. R.; Rnjak-Kovacina, J.; Li, C. M.; Isberg, R. R.; Kumamoto, C. A.; Mecsas, J.; Kaplan, D. L. Robust bioengineered 3D functional human intestinal epithelium. *Sci. Rep*. **2015**, *5*, 13708.

[167] Mayer, E. A. Gut feelings: The emerging biology of gut-brain communication. *Nat. Rev. Neurosci*. **2011**, *12*, 453–466.